INFORMATION TO USERS

This manuscript has been reproduced from the microfilm master. UMI films the text directly from the original or copy submitted. Thus, some thesis and dissertation copies are in typewriter face, while others may be from any type of computer printer.

The quality of this reproduction is dependent upon the quality of the copy submitted. Broken or indistinct print, colored or poor quality illustrations and photographs, print bleedthrough, substandard margins, and improper alignment can adversely affect reproduction.

In the unlikely event that the author did not send UMI a complete manuscript and there are missing pages, these will be noted. Also, if unauthorized copyright material had to be removed, a note will indicate the deletion.

Oversize materials (e.g., maps, drawings, charts) are reproduced by sectioning the original, beginning at the upper left-hand corner and continuing from left to right in equal sections with small overlaps.

Photographs included in the original manuscript have been reproduced xerographically in this copy. Higher quality 6" x 9" black and white photographic prints are available for any photographs or illustrations appearing in this copy for an additional charge. Contact UMI directly to order.

Bell & Howell Information and Learning
300 North Zeeb Road, Ann Arbor, MI 48106-1346 USA
800-521-0600

Université d'Ottawa · University of Ottawa

This thesis is dedicated with love

to my mother and sister

Abstract

This thesis represents the completion of two years of research in the field of gas-phase ion chemistry. A Finnigan GCQ ion trap mass spectrometer has been modified for the measurement of ion/molecule reaction rate constants. The rate constants for the reactions between $CH_3OH_2^+$ and methanol, $CH_3CH_2OH_2^+$ with methanol and ethanol, $CH_3CH_2CH_2OH_2^+$ with methanol, ethanol and n-propanol and protonated isopropanol with neutral isopropanol, all leading to products consisting of a protonated ether and neutral water, have been determined. All of the values, except that for the reaction involving isopropanol, are significantly lower than that predicted by the collision capture theory of Su and Chesnavich. Common to all the systems studied is an isomerization reaction that takes place in the proton-bound dimer that is initially formed in the reaction. This isomerization, which takes place via an internal S_N2-type mechanism, leads to the formation of the protonated ether. The rate constants, in combination with RRKM modelling, allow the isomerization activation energies, E_{iso}, for the proton-bound dimers to be estimated. The E_{iso} values decrease as the size of the alcohols increase, an observation consistent with the S_N2-type rearrangement that has been predicted for these systems.

The second portion of this work involved measuring the ion/molecule reaction rate constants for three reactions involving acetonitrile and primary alcohols. The value obtained for the reaction between CH_3CNH^+ and CH_3OH leading to the products $CH_3CNCH_3^+$ and H_2O was $(4.6 \pm 0.2) \times 10^{-11}$ cm^3 molecule^{-1} s^{-1}. The reaction between CH_3CNH^+ and CH_3CH_2OH (to give $CH_3CNCH_2CH_3^+ + H_2O$) proceeds with a rate constant of $(3.9 \pm 0.4) \times 10^{-10}$ cm^3 molecule^{-1} s^{-1},

while that between $CH_3CH_2CH_2OH_2^+ + CH_3CN$ has a value of $(2.1 \pm 0.4) \times 10^{-10}$ cm^3 $molecule^{-1}$ s^{-1}. These values for the rate constants have been used to extract the activation energy for isomerization of the initially formed proton-bound dimer in each case.

Acknowledgements

First of all, I would like to thank my supervisor, Dr. Paul Mayer, for his continuous support and guidance during the pursuit of this degree. I can't think of a better person with whom to have started my research career (even if he does drink coffee...) nor will I forget his never-ending patience when I know I must have been trying it. I also want to thank him for giving me the opportunity to present a poster at the Lake Louise Tandem Mass Spectrometry conference and for encouraging me to present posters and presentations even when I felt I couldn't do it. My experiences in his research group have taught me more than words can express.

Second of all, I want to thank my immediate family for their never-ending love and support, especially my mother who has always believed in me when I doubted myself. I also want to thank Mark, for being so supportive of the long hours needed to finish this degree (and the next one) and for always brightening my day, especially on the days that things didn't go quite as I had hoped. I truly feel blessed to have such loving people in my life.

What would a lab be without super people to work with? I would like to thank the graduate students and post-docs I have worked beside in the lab (in no particular order): Jie Cao (for her listening ear), Richard Ochran (for being a great guy to work with and a true friend), Don Dawson, Dr. Yaping Tu, Dr. WeiXing Sun, Dr. Natalia Vais, Dr. Vladimir Vais and Dr. Christiane Aubry (for her insightful words of wisdom and warm heart). I also want to

acknowledge the two undergraduates, Clement Poon and Danielle Dubien, who work in the lab. Lastly, I want to thank Dr. Clem Kazakoff, for his friendliness in the morning, Dr. Alexander Mommers (Sander) for his array of knowledge about mass spectrometers and Dan Lafleur, for always knowing how to make me smile.

In all, since this is longer than I had planned, I want to thank the University of Ottawa for financial support and Joseph Hui, Tammy Leriche, Marcel Beaudoin, and Rachel Mainville, for their friendship. My experiences here as a graduate student have taught me more than I can express.

Julie

Contents

List of Tables

List of Figures

List of Abbreviations

α	Polarizability
ρ_{cap}	Probability of Ion/Molecule Collision
μ	Reduced Mass
μ_D	Dipole Moment
a_z, q_z	Trapping Parameters
ADO	Average-Dipole Orientation
DC	Direct Current
GC	Gas Chromatograph
G2	Gaussian-2 Theory
HF	Hartree-Fock
ICR	Ion-Cyclotron Resonance
MI	Metastable Ion
MP	Moller-Plesset Pertubation Theory
MS	Mass Spectrometry
MS^2	Mass Spectrometry/Mass Spectrometry
m/z	mass-to-charge ratio
PA	Proton Affinity ($M + H^+ \rightarrow MH^+$ $\Delta H = -PA$)
RF	radiofrequency
RRKM/QET	Rice-Ramsperger-Kassel-Marcus/ Quasi-Equilibrium Theory
SIFT	Selected-Ion Flow Tube

S_N2	Secondary Nucleophilic Substitution
r_0	radius of the ring electrode in the central horizontal plane
$2z_0$	separation of the two end-cap electrodes measured along the axis of the ion trap

Chapter 1

Ion/Molecule Reactions and Cluster Ions

1.1 History of Ion/Molecule Reaction Chemistry

The mass spectrometer has proved to be one of the most flexible and useful of all scientific instruments. In the first quarter of the 20th century, mass spectrometers were used for chemical analysis, ionization and appearance energy measurements, atomic mass determination and the studies of ion/molecule reactions. Arguably, of all of these, ion/molecule reactions have provided information pertaining to the widest variety of applications [1].

The first ion/molecule reaction was discovered at the turn of the last century and involved the reaction between molecular and ionic H_2 to form H_3^+:

$$H_2^+ + H_2 \rightarrow H_3^+ + H$$

In 1913, J.J. Thompson, known as the father of mass spectrometry, identified the ion with m/z 3 as H_3^+[2], but the mechanism for the formation of this ion was not determined until 1925 [3,4].

Another landmark was the study of the auto-protonation of methane. The reaction $CH_4^+ + CH_4 \rightarrow CH_5^+ + CH_3$ was studied [5] and a rate constant in the neighbourhood of 10^{-9} cm^3 $molecule^{-1}$ s^{-1} was derived. The existence of a strongly bonded compound CH_5^+ was completely

unexpected and as such, led to an intensified interest in ion/molecule reactions. It was apparent from the low pressures and short times required for the reactions to be observed that their rate constants were very large, approximately 10^{-9} cm^3 $molecule^{-1}$ s^{-1} (i.e., 10^{12} M^{-1} s^{-1}). It seemed probable, at this time, that little or no activation energy was involved and as such, reactions must be exothermic to be detected. This, of course, did not mean that all ion/molecule reactions were exothermic or did not have an activation energy. However, the recognition that a reaction under these conditions had to be exothermic to be detected proved very useful in the identification of possible mechanisms.

The initial studies in the 1950s were performed by mass spectrometrists on commercially available instruments designed primarily for quantitative analysis of complex mixtures and in some instances for the determination of the heats of formation of ions. While these sector instruments were useful for detecting a number of reactions and measuring approximate values of rate constants, they quickly became obsolete and new and better methods of study needed to be developed.

While the early work employing open, single-source instruments was provocative, it was primarily important in showing the possibilities of the field. Consequently, much emphasis was placed on the design and construction of instruments that would be better suited to the solution of specific problems in ion/molecule reaction chemistry. At first, low energy techniques were used such as the flowing afterglow [6] and flow-drift tube [7]. However further progress was achieved by mass-spectrometric methods which permit the selective isolation of ions in the

selected-ion flow tube (SIFT) [8] or in tandem mass spectrometers with an intervening collision chamber, crossed-beam, and merging-beam [9]. Most recently, the possibility of trapping ions for variable reaction times has led to powerful and versatile methods, such as Fourier-Transform mass spectrometry [10] and ion trap mass spectrometry [11,12], as they enable the pathway and kinetics of gas-phase ion/molecule reactions to be evaluated. It is important to note, however, that although each of these instruments has proved useful for solving specific problems, none is suited for solving all problems.

1.2 Characteristic Features of Ion/Molecule Reactions

Another reason for the growth in interest in the chemistry and physics of ion/molecule reactions is their ease of study. Ions, because of their electric charge, are more easily manipulated and detected than neutrals. As such, fewer ions are required for detection and quantitative measurement. Another interesting fact is that the cross-section for an ion/molecule collision is usually an order of magnitude greater than that for two neutrals of similar mass [13]. Because of this, collision reactions of ions and neutrals can be readily studied at very small concentrations of reactants.

Characteristic values of the rate constants of ion/molecule reactions are on the order of 10^{-9} to 10^{-10} cm^3 $molecule^{-1}$ s^{-1}, close to the collision rate constant [14,15]. The latter is calculated by the Langevin formula in the case of ion/nonpolar molecule collisions, but by more complicated treatments when the molecule is polar. The classical Langevin type treatments

employ only large values of cross sections of ion/molecule reactions; they have nothing to do with the problem of chemical bond rearrangement. The low (or non-existent) activation energy is due to the presence of the electric charge in the system of colliding particles. These theories and concepts will be discussed in detail in the forthcoming chapter.

Exothermic and thermoneutral ion/molecule reactions are usually extremely fast processes. Based on early experiments of ion/molecule reactions in hydrocarbon gas mixtures, Talrose and Lyubimova [15] suggested that exothermic and thermoneutral reactions, for the most part, would have no noticeable activation energy and would proceed on each collision. The most interesting of these features is the fact that they proceed with such a high rate constant that in most cases, the reactions carry on practically at each collision by one of several possible exothermic channels. At that time, this notion was rather surprising since kineticists knew that even in fast reactions of neutral particles (not including radicals), there was a significant activation energy. Such a difference between the reactions of neutral particles and ion/molecule reactions is qualitatively connected with the presence of electric charge in the system. Subsequent experiments by other authors confirmed the accuracy of this suggestion for many types of ion/molecule reactions.

As information accumulated on ion/molecule reactions, comparatively slow ion/molecule reactions were discovered in a small percentage of cases. Slow processes are referred to those reactions whose rate constants are less than 10^{-10} cm^3 $molecule^{-1}$ s^{-1} or whose cross sections are more than one order of magnitude less than the Langevin value. One of the first "slow" reactions

was observed by Giese and Meier in 1962 [16] and is shown below.

$$He^+ + H_2 \rightarrow HeH^+ + H \qquad k \leq 10^{-13}\ cm^3\ molecule^{-1}\ s^{-1}.$$

These "slow" reactions were also exothermic, and so factors other than reaction thermochemistry were found to play a role in determining the reaction rate constant. In some cases, an approach based on orbital symmetry conservation rules (i.e., Woodward and Hoffman rules [17]) turned out to be valuable for the qualitative estimation of ion/molecule reaction rates. These rules suggest that a reaction occurs easily when there is a relationship between the orbital symmetry of reagents and reaction products. Experimental data indicate that the majority of symmetry-allowed reactions have rate constants higher than 10^{-11} cm^3 $molecule^{-1}$ s^{-1} and in a number of symmetry-forbidden reactions, they are slower. To apply these rules to chemical kinetics, it is necessary to determine the rate constant range for symmetry-allowed and symmetry-forbidden reactions. Such a qualitative approach proved to be successful in the prediction of the likelihood of the occurrence of certain organic reactions. Another factor that can affect an ion/molecule reaction rate constant is cluster ion isomerization.

1.3 Ion/molecule Reactions and Cluster Ion Chemistry

Generally, every ion/molecule reaction involves a cluster ion. A cluster ion consists of an ion, A^+ and a molecule, B, which are bound together electrostatically. This ion can then go on to form additional products, as shown below.

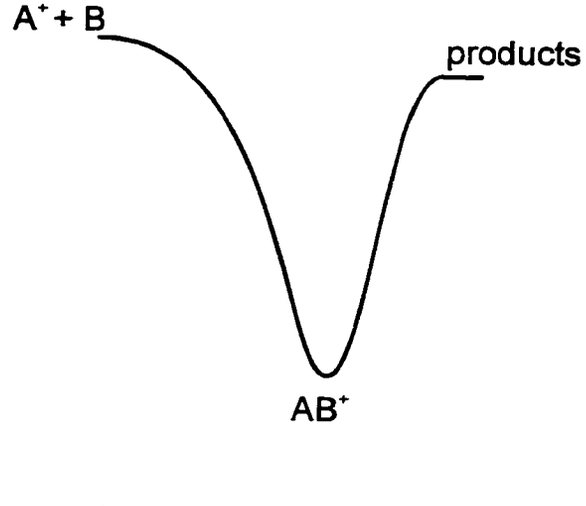

From this diagram, we can see that cluster ion chemistry and ion/molecule reaction mechanisms and kinetics are inextricably linked. Knowledge obtained about one affects our understanding of the other.

Cluster ions are viewed as an intermediate state of matter between the dilute gas phase and solution [18] and they can range in size from simple dimers such as H_2^+ to relatively large poly-molecular species such as water hydrates, $H_3O^+(H_2O)_n$. A family of cluster ions that has received considerable attention is the family of proton-bound dimers and one of the main reasons for this interest is the role they play in atmospheric chemistry [19]. A change in the ion chemistry of the atmosphere is observed as the altitude decreases; it goes from being dominated by the atomic and diatomic ionization products of N_2 and O_2 (above ca. 90 km) [20] to a complex ensemble of water hydrate clusters, $(H_2O)_nH^+$ [21,22].

A central issue when studying the chemistry of any gaseous ion is their propensity for rearrangement prior to reaction. Over the years, a variety of thermodynamically stable structures

have been discovered that play key roles in ion dissociation mechanisms, including distonic ions (such as $^{\bullet}CH_2OH_2^+$) [23] and bridged ions (such as $[CH_3CO\bullet\bullet\bullet H\bullet\bullet\bullet OCH_2]^+$) [24]. The isomerization of more conventional organic ions has been extensively studied, while the isomerization of cluster ions has not. In the reaction surface shown above, the formation of products from AB^+ may only proceed after the isomerization of the dimer. Thus, the kinetics of the ion/molecule reaction will reflect this isomerization process.

Useful information which can be obtained for a potential energy surface is thus the isomerization barrier energy, E_{iso}, of the cluster ion AB^+. While theoretical methods can be used to calculate transition structures and determine E_{iso}, accurate results are difficult to obtain for large systems. In this work, E_{iso} was extracted for various alcohol-nitrile and alcohol-alcohol proton-bound dimers by using the rate constants obtained with the Finnigan GCQ ion trap mass spectrometer.

1.4 Aim of this thesis

This thesis comprises two years of gas-phase ion chemistry research done using mass spectrometry. There were two central goals to this work: to develop an ion trap mass spectrometer as a tool to measure rate constants and to extract, from the kinetic data, values for the isomerization energy barriers of proton-bound dimers.

References

[1] J. L. Franklin, *Ion-Molecule Reactions*; J. J .Kaufman and W. S. Koski (Ed), Dowden, Hutchinson and Ross, Pennsylvania, 1979; Vol. 3.

[2] J. J. Thompson, Rays of positive electricity, Longman, Green and Company, Essex, 1913.

[3] H. D. Smyth, Phys. Rev. 25 (1925) 452.

[4] T. R. Hogness and E. G. Lunn, Phys. Rev 26 (1925) 44-55.

[5] V. L. Talrose and A. K. Lyubimova, Dokl. Akad. Nauk SSSR 86 (1952) 909-912.

[6] E. E. Ferguson, F. C. Fehsenfeld and A. L. Schmeltekopf, Adv. At. Mol. Phys. 5 (1969),1.

[7] M. McFarland, D. L. Albritton, F. C. Fehsenfeld, E. E. Ferguson and A. L. Schmeltekopf, J. Chem. Phys 59 (1973) 6610-6619.

[8] N. G. Adams and D. Smith, Int. J. Mass Spectrom. Ion Phys. 21 (1976) 349-359.

[9] B. S. Freiser, in Techniques for the Study of Ion-Molecule Reactions, J. M. Farrar and W. H. Saunders (Ed),Wiley-Interscience, New York, 1988.

[10] J. M. Farrar, in Techniques for the Study of Ion-Molecule Reactions, J. M. Farrar and W. H. Saunders (Ed), Wiley-Interscience, New York, 1988.

[11] R. E. March and J. F. J. Todd *Practical Aspects of Ion Trap Mass Spectrometry*; CRC Press: Boca Raton, 1995.

[12] R. E. March, J. Mass Spectrom. 32 (1997) 351-369.

[13] G. Gioumousis and D. P. Stevenson, J. Chem. Phys 29 (1958) 294-299.

[14] D. O. Schissler and D. P. Stevenson, J. Phys. Chem. 24 (1956) 926.

[15] V. L. Talrose, P. S. Vinogradov and I. K. Larin, in Gas-phase ion chemistry, M.T.

Bowers (Ed), Academic Press, New York,1979.

[16] C. F. Giese and W. B. Meier, J. Chem. Phys. 35 (1961) 1913.

[17] R. Woodward and R. Hoffman, J. Am. Chem. Soc. 87 (1965) 395.

[18] P. Kebarle, in Techniques for ion-molecule reactions, J. M. Farrar and W. H. Saunders (Ed), Wiley-Interscience, New York, 1988.

[19] E. E. Ferguson, F. C. Fehsenfeld and D. L. Albritton, in Gas Phase Ion Chemistry, M. T. Bowers (Ed), Academic Press, New York, 1979.

[20] D. Smith and P. Spanel, Mass Spec. Rev. 14 (1995) 255.

[21] E. Arijs, J. Ingels and D. Nevejans, Nature 288 (1980) 684.

[22] E. Arijs, J. Ingels and D. Nevejans, Nature 271 (1978) 642.

[23] B. F. Yates, W. J. Bouma and L. Radom, Tetrahedron 22 (1986) 6225.

[24] N. Heinrich and H. Schwarz, in Ion and Cluster Ion Spectroscopy, Elsevier, Amsterdam, 1989.

Chapter 2

Theory

2.1 Introduction

The history of the ion trap dates back to the pioneering work of Paul and Steinwedel, which was recognized by the presentation of the shared award of the 1989 Nobel Prize for Physics to Wolfgang Paul [1]. A patent of the quadrupole ion trap was filed in 1953 where it was described as "still another electrode arrangement" and it was within this patent that the operating principle of the quadrupole mass spectrometer was first described [2]. The characterization of the ion trap developed in the 1960s and 1970s, but it was the announcement by Finnigan MAT in 1983 of a novel scanning technique for the ion trap detector, by which a mass spectrum of stored ions could be acquired, that began a new era in mass spectrometry [3].

2.2 Quadrupole Ion Trap

The quadrupole ion trap is a three dimensional instrument, which functions both as an ion storage device in which gaseous ions can be confined for a period of time and as a mass selective device in the form of a mass spectrometer. Both of these functions are enhanced by the presence of 1 mTorr of helium buffer gas [3-5].

The ion trap consists of three cylindrically symmetric electrodes, two end-caps and a ring.

Each electrode has accurately machined hyperbolic internal surfaces and in the normal mode of use, the end-cap electrodes are grounded while an ca. 1 MHz radiofrequency (RF) oscillating potential is applied to the ring electrode. Ions can either be formed in the trap by electron impact ionization or can be formed externally and injected into the trap. By manipulating the RF potential, a range of mass to charge (m/z) values may be held in bound (or stable) orbits (i.e., kept within the confines of the trap). As the amplitude of the RF potential is increased, the motion of ions in the trap becomes progressively more energetic such that the ions eventually develop unstable trajectories along the z-axis and are thus ejected from the potential well. Each ion species is ejected from the potential well at a specific RF amplitude and because the initial amplitude and ramping rate are known, the m/z ratio of each ion species can be determined upon ejection. The stability of an ion within the trap is explained in terms of the "mass-selective axial instability mode" developed by Stafford [6] and it is this discovery that made possible the commercialization of the quadrupole ion trap in the early 1980s.

2.2.1 The Structure of the Quadrupole Ion Trap

As mentioned in the previous section, the quadrupole ion trap consists of three electrodes, which are hyperbolic in geometry, two end-cap electrodes and a ring electrode. The entrance end-cap electrode has a single aperture through which electrons and/or ions are gated periodically while the exit end-cap electrode typically has several small apertures, arranged centrally, through which ions pass to a detector. In ion trap instruments with external ion sources, such as the Finnigan GCQ, each end-cap electrode only has a single perforation. The third electrode, also of hyperbolic geometry, is a ring electrode positioned symmetrically between

the two end-cap electrodes. Fig.2.2.1 is a cross-sectional view of a quadrupole ion trap electrode structure showing the dimensions r_0 and z_0 where r_0 is the radius of the ring electrode in the central horizontal plane and $2z_0$ is the separation of the two end-cap electrodes measured along the axis of the ion trap.

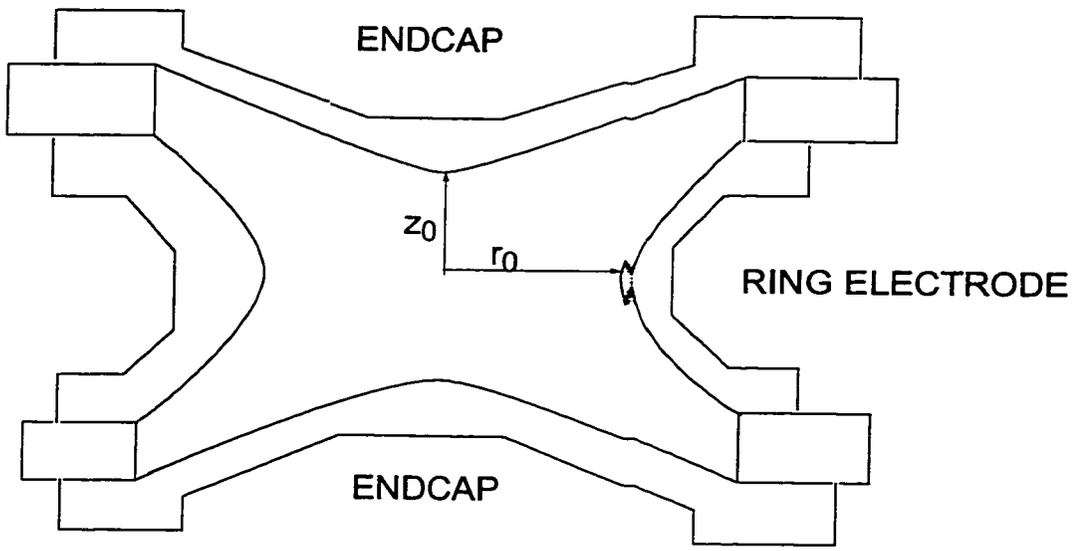

Fig. 2.2.1 Cross-section of the quadrupole ion trap

The geometries of the electrodes are defined in such a manner to produce an ideal quadrupole field which will, in turn, produce a parabolic potential well for the confinement of ions. For an ideal quadrupole field, the identity $r_0^2 = 2z_0^2$ must be satisfied so that once the magnitude of r_0 is given, the sizes of all three electrodes and the electrode spacings are fixed. The ratio of $z_0^2 : r_0^2$, however, is not necessarily restricted to 2 [7]. Regardless of the value of this ratio, the size of the ion trap is determined largely by the magnitude of r_0 and in the majority of commercial ion traps used today, r_0 is either 1.00 cm or 0.707 cm. The Finnigan GCQ ion trap

employed for all the experiments described in this thesis has a r_0 value of 0.707 cm.

2.3. An Ion in a Quadrupole Field

An ion in a quadrupole field experiences strong focussing in that the restoring force, which drives the ion back towards the centre of the device, increases as the ion deviates from the centre. The motion of ions in a quadrupole field can be described mathematically by the solutions to the second-order linear differential equation described originally by the Mathieu Equation [8].

The commonly accepted form of the Mathieu Equation is:

$$\frac{d^2u}{d\xi^2} + (a_u - 2q_u\cos 2\xi)u = 0 \qquad (2.4.1)$$

where u represents the co-ordinate axes x,y and z, ξ is a dimensionless parameter equal to $\Omega t/2$ such that Ω must be a frequency as t is time, and a_u and q_u are additional dimensionless parameters known as trapping parameters. Ω will reappear later as the radial frequency (in rad/s) of the RF potential applied to the ring electrode. Through some mathematical manipulations, it can be shown that

$$m\frac{d^2u}{dt^2} = \frac{-m\Omega^2}{4}(a_u - 2q_u\cos\Omega t)u \qquad (2.4.2)$$

whereby the left-side represents the force on an ion (i.e., mass times acceleration) in each of the three co-ordinate directions.

Since the field in quadrupole devices is uncoupled, the forces in the three co-ordinate directions can be determined separately. For simplicity, only the force experienced by an ion of mass m and charge e at any point within a quadrupole field in the x-direction, F_x, will be considered.

$$F_x = ma = m\frac{d^2x}{dt^2} = -e\frac{\partial\phi}{\partial x} \qquad (2.4.3)$$

where a is the acceleration of the ion, e is the electronic charge and ϕ is the potential at any point (x,y,z) within the field. Similar expressions for F_y and F_z can be obtained. It should be noted that this equation relates the force on an ion to the field within the trap.

The quadrupole potential ϕ can be expressed as

$$\phi = \frac{\phi_o}{r_o^2}(\lambda x^2 + \sigma y^2 + \gamma z^2) \qquad (2.4.4)$$

where ϕ_0 is the applied electric potential, λ,σ and γ are weighting constants for the x,y and z co-ordinates respectively and r_o is a constant which is defined separately depending on whether the quadrupole device is an ion trap or mass filter.

Through several mathematical manipulations of eq. (2.4.4) as shown in Quadrupole Mass Spectrometry by R.E. March [4], it has been shown that the potential at any point within the quadrupole field in a quadrupole ion trap can be represented by

$$\phi_{r,z} = \frac{\phi_o}{r_o^2}(r^2 - 2z^2) \tag{2.4.5}$$

The applied electric potential, ϕ_0 (that is, applied to the ring electrode) is either an RF potential $V\cos\Omega t$ or a combination with a DC potential, U, of the form

$$\phi_o = U + V\cos\Omega t \tag{2.4.6}$$

When an expression for ϕ_0 as given by eq. (2.4.6) and λ =1 are substituted into eq.(2.4.4) and ϕ is differentiated with respect to x, the following expression is obtained.

$$\frac{\partial\phi}{\partial x} = \frac{2x}{r_0^2}(U + V\cos\Omega t) \tag{2.4.7}$$

which when substituted into eq. (2.4.3) yields an expression for the force on an ion

$$m\frac{d^2x}{dt^2} = \frac{-2e}{r_0^2}(U + V\cos\Omega t)x \tag{2.4.8}$$

At this point, the terms on the right hand sides of eqs. (2.4.2) and (2.4.8) can be directly compared, recalling that u represents x, to obtain

$$a_x = \frac{8eU}{mr_o^2\Omega^2} \qquad q_x = \frac{-4eV}{mr_o^2\Omega^2} \tag{2.4.9}$$

For the quadrupole ion trap, it has been found that $q_x=q_y$.

$$a_z = \frac{-8eU}{mr_o^2\Omega^2} \qquad q_z = \frac{4eV}{mr_o^2\Omega^2} \tag{2.4.10}$$

Since most commercial ion trap instruments (including the GCQ) do not offer the flexibility of applying a DC potential to the electrodes, a_z will be ignored (i.e., $a_z=0$). As a result, the most common mode of ion trap operation corresponds to operation on the z-axis. The expression for q_z in eq.(2.4.10) contains the m/z ratio for a given ion, the size of the ion trap, r_0, the amplitude V of the RF potential and the radial frequency Ω; that is, all of the parameters which are necessary in order to understand the various operations of the ion trap.

2.3.1 The "Stretched" Ion Trap

The electrodes of the ion trap are truncated in order to obtain a practical working instrument, but this truncation introduces higher order multipole components to the potential, $\phi_{z,r}$. Because of this truncation, $r_0^2 \neq 2z_0^2$. In order to compensate for the stretching of the ion trap electrodes, the trapping parameters are now calculated using the actual values of z_0 and r_0 and are shown below in eqs. (2.4.11) and (2.4.12).

$$a_r = \frac{8eU}{m(r_o^2+2z_o^2)\Omega^2} \qquad q_r = \frac{-4eV}{m(r_o^2+2z_o^2)\Omega^2} \tag{2.4.11}$$

and $$a_z = \frac{-16eU}{m(r_o^2 + 2z_o^2)\Omega^2} \qquad q_z = \frac{8eV}{m(r_o^2 + 2z_o^2)\Omega^2} \tag{2.4.12}$$

When $r_0^2 = 2z_0^2$ is substituted into eq. (2.4.12), we obtain the trapping parameters listed in eq. (2.4.10). The geometry for the GCQ ion trap (i.e., stretched geometry) has an r_0 value of 0.707 cm and a z_0 value of 0.785 cm so that the geometry is stretched by 57%.

2.4 Regions of Ion Trajectory Stability

The operation of a quadrupole ion trap is concerned with the experimental conditions that determine whether an ion is stored or ejected from the device and if it is ejected, then whether it is lost or detected externally. It is these principles upon which the mass-selective stability diagrams are prepared and depict the stability of the trajectory of an ion within the field.

There are two types of solutions to Mathieu's equation: periodic but unstable and periodic and stable. The unstable solutions, often referred to as Mathieu functions of integral order, form the boundaries of unstable regions on the stability diagram. These boundaries correspond to those values of a new trapping parameter, β_z, which are integers (i.e. 0,1,2,3...). β_z is a complex function of a_z and q_z. Essentially, the boundaries represent the point at which the trajectory of an ion becomes unstable.

The stable solutions determine the motion of ions in an ion trap. Ions can be stored in

the ion trap provided that their trajectories are stable in the r- and z-directions, simultaneously. This stability is plotted in a_z,q_z space and shown in Figure 2.4.1.

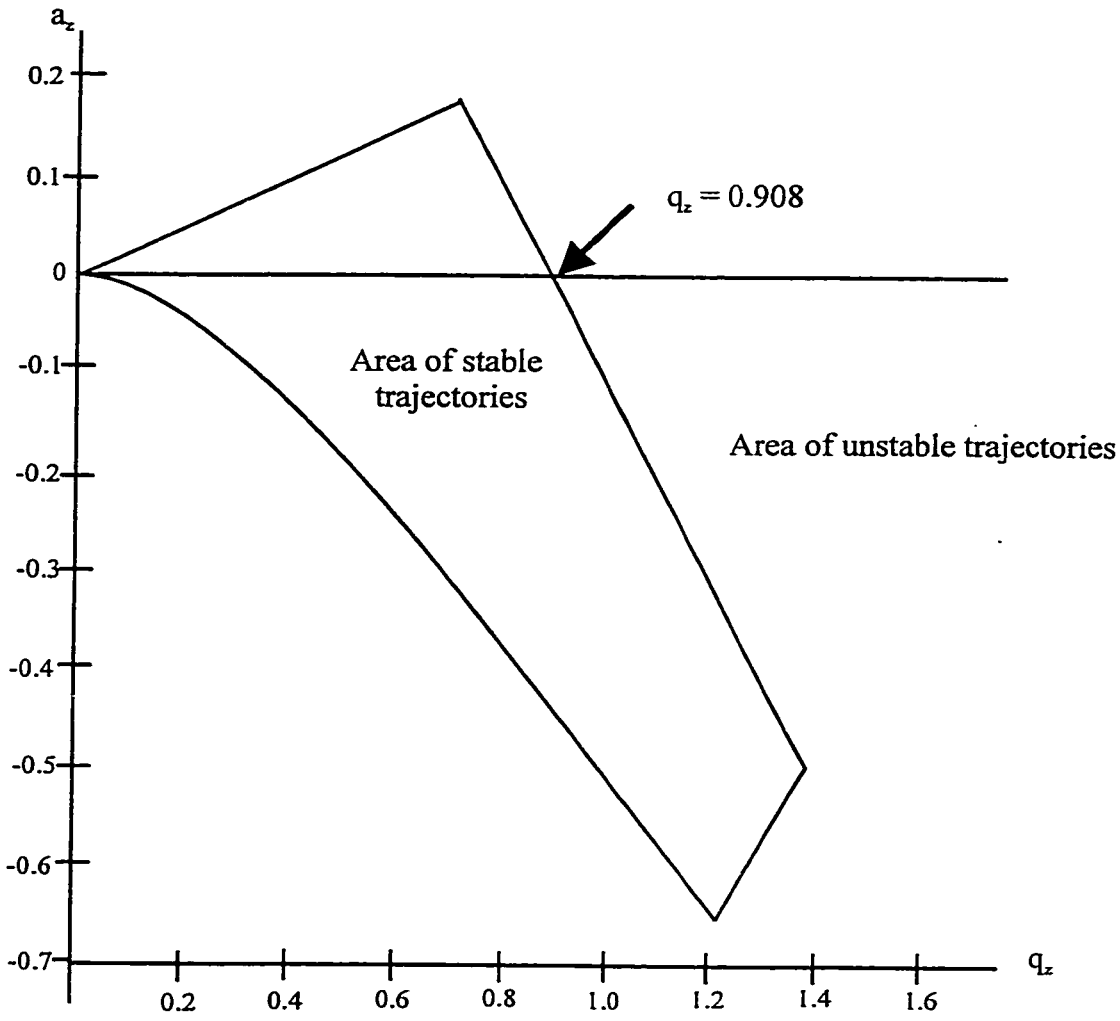

Figure 2.4.1 Portion of the Stability Diagram for motion of ions in a 3-D quadrupolar field, near the centre of the trap (region most of interest to operation of the instrument).

2.5 Resonant Excitation

Since the motion of ions confined in a quadrupole ion trap is characterized by both axial and radial frequencies, ion motion can be excited upon resonant irradiation at either or even both of these frequencies. This is called resonant excitation and is achieved by applying a small supplementary oscillating potential of a few hundred millivolts across the end-cap electrodes. Resonant excitation has become a powerful technique in quadrupole ion trap mass spectrometry owing to the use of predetermined waveforms composed of specified frequencies or frequency ranges. However, prior to resonant excitation of ion trajectories, ions first must be focussed to the centre of the trap under the influence of collisions with helium buffer gas. This process is referred to as ion cooling in that ion kinetic energies are reduced to ca. 0.1 eV, which in turn, corresponds to ca. 800 K (as calculated from $3RT/2 = 0.1$ eV). The resonant excitation of these cooled ions causes the ions to deviate from the centre of the trap so that they experience a greater trapping field. This process of ion excitation is often referred to as "tickling". These ions are then accelerated further by the trapping field such that they can achieve kinetic energies of tens of electronvolts.

There are various uses for resonant excitation in ion trap mass spectrometry [4], of which only the most important will be discussed. Its principal role is to remove unwanted ions during ionization in order to isolate a narrow range of m/z ratios. In this case, frequencies are applied to the end-cap electrodes to excite and eject many ions simultaneously leaving a single ion species isolated within the trap. Another important purpose is to excite the ions and cause their

kinetic energy to increase. This increase in ion kinetic energy promotes endothermic ion/molecule reactions, deposits internal energy in ions through momentum-exchange collisions with helium atoms so that they dissociate, and causes ions to escape from the trapping potential and be ejected.

Various ac voltages are applied to the ring and end-cap electrodes to trap and eject ions according to their mass-to-charge ratios. These ac voltages, referred to as the main RF voltage, waveform voltage, resonance excitation RF voltage, and resonance ejection RF voltage are discussed below.

2.5.1 RF Voltage

An ac voltage of constant frequency (1.03 MHz) and variable amplitude (0 to 8500 V zero-to-peak) is applied to the ring electrode by a spring-loaded pin that contacts the ring electrode when the mass analyzer is in place. The frequency of the ac voltage is in the RF range, and this voltage is referred to as the main RF voltage. The application of an RF voltage to the ring electrode produces a three-dimensional quadrupole field within the ion trap mass analyzer cavity. This time-varying field drives ionic motion in both the axial (toward the end-caps) and radial (toward the ring electrode) directions. For an ion to remain trapped, this ionic motion must be stable in both the axial and radial directions.

When the amplitude of the main RF voltage is low, all ions above a minimum mass are

trapped; this RF voltage is referred to as the storage voltage. During mass analysis, the main RF voltage is ramped at a constant rate corresponding to approximately 10,000 u s^{-1}. As the main RF voltage increases, ions of increasing mass become successively unstable in the axial direction such that they are ejected from the mass analyzer. The ejection of ions of each m/z ratio occurs over a short period of time and the voltage at which each ion is ejected from the mass analyzer is defined as its resonance voltage.

2.5.2 Waveform voltages

The waveform voltages consist of a distribution of frequencies between 10 and 400 kHz containing all resonance frequencies except those corresponding to the ions to be trapped. There are two types of waveform voltages, ionization waveform voltage and isolation waveform voltage.

The ionization waveform voltage acts during the ionization (and ion storage) step to eject ions present at the low end and high end of the mass range whereas the isolation waveform voltage acts during the isolation step of the MS/MS application. The isolation waveform voltage, in combination with the main RF voltage, ejects all ions except those of the selected mass or narrow range of masses and is calculated by the data system and automatically applied at the correct time.

During the collision-induced step of the MS/MS application, the resonance excitation RF

voltage is applied to the end-cap electrodes to fragment parent ions into product ions. The resonance excitation RF voltage is not strong enough to eject an ion from the trap, but does serve to enhance the ion motion in the axial direction, so that the ion gains kinetic energy. After many collisions with the helium buffer gas, the ion gains enough internal energy to dissociate into product ions. The product ions are then stored and mass analyzed. In our experiments, we only store ions, therefore, we keep this voltage at zero.

During mass analysis, the resonance ejection RF voltage facilitates the ejection of ions from the mass analyzer, which in turn, improves mass resolution. This voltage is applied at fixed frequency and increasing amplitude during the ramp of the main RF voltage on the ring electrode. Only when an ion is about to be ejected from the mass analyzer cavity is it in resonance with this frequency. When an ion comes into resonance, it moves away from the centre of the trap, where the field generated by the ring electrode RF voltage is zero into a region where the field is strong. As a result, the ejection of the ion is facilitated.

2.5.3 Helium Damping Gas in the Mass Analyzer Cavity

As previously mentioned in section 2.5, the mass analyzer cavity contains helium that is used as a damping gas. The helium damping gas enters the mass analyzer cavity through a nipple on the entrance end-cap electrode. The flow of gas into the mass analyzer cavity is regulated by a pressure regulator and a capillary restrictor, while the flow of gas out of the mass analyzer cavity (and into the diffusion pump) is restricted by the small holes in the end-cap electrodes.

Both of these flows are matched so that the partial pressure of helium in the mass analyzer cavity is maintained at approximately 1 mTorr.

The presence of helium in the trap significantly enhances sensitivity and mass spectral resolution. Before their ejection from the mass analyzer cavity, sample ions collide with helium atoms to reduce the kinetic energy of the ions. As a result, the ions are focussed into the center of the cavity rather than being spread throughout the cavity. Another function of the helium buffer gas is to slow the ions through third-body collisions so that the ions are more easily trapped by the RF fields.

As mentioned in the previous section, helium in the cavity also acts as a collision gas. During the collision induced dissociation step of an MS/MS experiment, the resonance excitation RF voltage applied to the end-cap electrodes drives parent ions into the helium atoms. After gaining sufficient internal energy from the resulting collisions, a parent ion dissociates into one or more product ions.

2.6 Kinetics of Ion/Molecule Reactions

Chemical kinetics involves the study of the rates of chemical reactions and the mechanisms by which they proceed. The quadrupole ion trap mass spectrometer serves as a tool for measuring the bimolecular rate constants of ion/molecule reactions. In general, when an ion, A^+, reacts with a neutral, B, the first step is to form an excited dimer ion, $(AB^+)^*$ [9]. This

excited dimer ion then can undergo a variety of competing processes, as summarized in Figure 2.6.1.

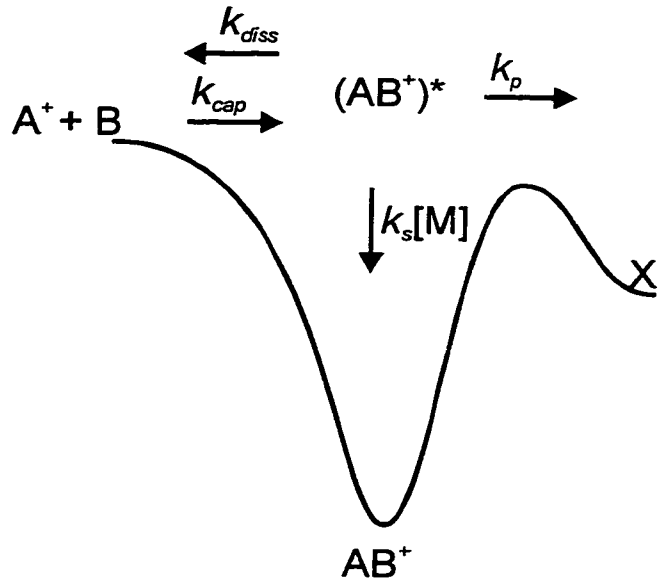

Figure 2.6.1. General Surface for an Ion/Molecule Reaction

where A^+ and B are reactants.

X is(are) the product(s) of the reaction.

$(AB^+)^*$ is the reactive excited intermediate dimer ion.

k_{cap} is the rate constant for capture collisions between the reactant ion and neutral.

$k_s[M]$ is the rate constant for collisional stabilization of the initially formed excited dimer ion.

k_{diss} is the rate constant for the dissociation of the initially formed excited dimer ion.

k_p is the rate constant for the isomerization reaction of the initially formed excited dimer ion.

We are interested in investigating the rate of formation of products and thus dX/dt. Therefore, we wish to derive an expression such that

$$\frac{dX}{dt} = k_p\left[\left(AB^+\right)^*\right] \qquad (2.6.1)$$

Using the steady-state approximation, we get:

$$\frac{d[(AB^+)^*]}{dt} = k_{cap}[A^+][B] - k_{diss}[(AB^+)^*] - k_s[M][(AB^+)^*] - k_p[(AB^+)^*] = 0 \quad (2.6.2)$$

Isolating $[(AB^+)^*]$ from the above equation,

$$[(AB^+)^*] = \frac{k_{cap}[A^+][B]}{k_{diss} + k_s[M] + k_p} \quad (2.6.3)$$

yields an expression for dX/dt:

$$\frac{dX}{dt} = \frac{k_p k_{cap}[A^+][B]}{k_{diss} + k_s[M] + k_p} \quad (2.6.4)$$

which can be written as $$\frac{dX}{dt} = k_{obs}[A^+][B] \quad (2.6.5)$$

where $$k_{obs} = \frac{k_p k_{cap}}{k_{diss} + k_s[M] + k_p} \quad (2.6.6)$$

Since $[B] >> [A^+]$ at any given moment, the reaction can follow pseudo-first order kinetics.

i.e. $v = k'[A^+]$ where $k' = k_{obs}[B]$

By plotting ln $([A^+]_t / [A^+]_o)$ vs. time, a straight line is obtained yielding a value for k'.

By plotting k' vs. [B], which is the pressure of the neutral, a value for k_{obs} is obtained.

2.6.1 Collision Theories

The above treatment provides us with an experimental determination of the ion/molecule reaction rate constant (k_{obs}). It is often useful in kinetics to compare the experimental reaction rate constant with theory. In the early development of chemical kinetics, it was often assumed that bimolecular reactions occur upon the first encounter of the reactants. Although it is now known that this assumption is usually not true, the concept of a "collision" or "capture" rate still serves in establishing an upper limit to measured rate constants. Numerous theories evolved over the course of the 20th century, each theory being a notable improvement over the previous one. There are in particular two collision theories which are most commonly used in the study of ion/molecule reactions, Langevin's classical impact parameter treatment [10] and Su and Chesnavich's parametrization model of ion/polar molecule collision rate constants by trajectory calculations [11].

The first theoretical paper relevant to the rates of ion/molecule reactions was published by Paul Langevin in 1905 [10], considerably before the identification of this type of reaction. This work is a classical impact parameter treatment assuming point-charge particles approaching each other at low velocities. In his treatment, the long-range potential between the ion and molecule was

$$V_L(r) = \frac{-1}{2}\left(\frac{\alpha q^2}{r^4}\right) \qquad (2.6.7)$$

where q is the unit of electron charge, r is the distance between the ion and centre of mass of the neutral and α is angle-averaged polarizability of the neutral. Thus, the expression derived for the capture reaction rate constant, k_{cap}, was

$$k_{cap} = 2\pi q\left(\frac{\alpha}{\mu}\right)^{1/2} \tag{2.6.8}$$

where μ is the reduced mass of the colliding pair. Langevin's theory was a step in the right direction, but limiting, as it was only valid for molecules without permanent dipole moments (i.e., non-polar). As a result, it was only natural that the theory would be extended to include the effect of a permanent dipole. Sixty years later, the theory was modified by Moran and Hamill [12] to account for molecules having a permanent dipole moment (μ_D) and so the equation became:

$$k_{cap} = 2\pi q\left[\left(\frac{\alpha}{\mu}\right)^{1/2} + \frac{\mu_D}{\mu v}\right] \tag{2.6.9}$$

where v is the relative velocity of the ion at infinite separation. At thermally averaged velocities, the rate constant becomes

$$\overline{k} = \frac{2\pi q}{\mu^{1/2}}\left[\alpha^{1/2} + \mu_D\left(\frac{2}{\pi k_B T}\right)^{1/2}\right] \tag{2.6.10}$$

This theory assumed that the dipole of the neutral was in perfect alignment with the field

of the charge. It was realized by many that this was an extreme case, and in the 1970s, Su, Chesnavich and Bowers [13] directed their attention to this problem. Their work proved to be fruitful providing results that were a considerable improvement over the fixed dipole treatment. They extended the previous theory to take into consideration the thermal rotational energy of the polar molecule and to adequately account for the effect of the permanent dipole moment on the rate constant. As a result, the average-dipole-orientation (ADO) theory was born [14].

The next and final advancement thus far is the theory developed by Su and Chesnavich [11] in 1982 to parametrize ion/polar molecule collision rate constants by trajectory calculations. This method is used to calculate the collision capture rate constants presented in this thesis. In their study, they treated the ion as a point charge, the polar molecule as a two-dimensional rigid rotor and assumed that an interaction potential of the form

$$V(r,\theta) = \frac{-\alpha q^2}{2r^4} - \frac{q\mu_D}{r^2}\cos\theta \qquad (2.6.11)$$

occurs where θ is angle that the dipole makes with r. It was shown by Chesnavich, Su and Bowers that the ratio of $k_{cap}(T)$ to the Langevin capture rate constant k_L depends only on two reduced parameters, the reduced temperature T_R and I*.

$$\frac{k_{cap}(T)}{k_L} = K_{cap}(T_R, I^*) \qquad (2.6.12)$$

where $T_R = 2\alpha k_B T/\mu_D^2$ and $I^* = \mu_D I/\alpha q\mu$ where I is the moment of inertia.

A trajectory study was done to determine the dependence of T_R and I* on the rate constant. It was found that K_{cap} is insensitive to I* at low values of I* and this insensitive region ends at lower I* as $1/(T_R)^{½}$ decreases. As I*→∞, K_{cap} falls to the "adiabatic limit". Since the adiabatic limit can be calculated exactly by transition state theory, the nearly identical values between K_{cap} as I*→∞ and the adiabatic rate constant demonstrate that the trajectory calculations are quite accurate. For most physically realistic systems, T_R and I* lie in this insensitive region, which can be defined to a good approximation by the empirical formula

$$I^* \prec \frac{0.7 + x^2}{2 + 0.6x} \tag{2.6.13}$$

where $x=1/(T_R)^{½}$. The empirical fit of the trajectory curve is

$$K_{cap} = 0.4767x + 0.6200 \text{ for } x \geq 2 \tag{2.6.14}$$

$$= \frac{(x+0.5090)^2}{10.526} + 0.9754 \text{ for } x \leq 2$$

Thus, by knowing the polarizability and dipole moment of the neutral, a value for $K_{cap}(T_R,I^*)$ can be determined and by multiplying this value by the Langevin rate constant, a value for k_{cap} can be derived.

2.6.2 RRKM Theory

The above treatment deals with the estimation of bimolecular ion/molecule reaction rate constants. In Fig. 2.6.1, the initially formed complex AB^+ can undergo the unimolecular reactions of dissociation to $A^+ + B$, and reactions leading to products, X. To model these processes, we employed the statistical theory [15] developed by Rice,Ramsperger,Kassel and Marcus (RRKM).

The RRKM equation, which yields the rate constant for a molecule at a given energy E and with an activation energy, E_0, is given by

$$k(E) = \frac{\sigma N^{\neq}(E - E_0)}{h\rho(E)} \qquad (2.6.15)$$

where σ is the reaction degeneracy, $N^{\ddagger}(E\text{-}E_0)$ is the transition-state sum of states from 0 to $E\text{-}E_0$, h is Planck's constant and $\rho(E)$ is the reactant ion density of states at energy E. There are several ways in which to calculate the sums and densities of states. The method employed for these studies is the direct count method developed by Beyer and Swinehart [16,17]; a simple Fortran 77 program was used to calculate these functions.

The vibrational frequencies of the reactant ion and the transition state give the entropy of activation $\Delta S^{\ddagger}$. The $\Delta S^{\ddagger}$ is a convenient way to describe the nature of the reaction and typically, values are reported at either 600 or 1000 K. For these studies, all $\Delta S^{\ddagger}$ values quoted are for 600 K. Transition states that are less ordered than the reactant ion are referred to as

"loose" and are characterized by positive $\Delta S^{\ddagger}$ values. Simple bond cleavage reactions typically have loose transition states. Conversely, transition states that are more ordered than the reactant ion are known as "tight" and have negative $\Delta S^{\ddagger}$ values. These transition states are usually associated with rearrangement processes. If the vibrational frequencies of the reactant ion and the transition state are known, then the nature of the process can be deduced. On the other hand, if the nature of the process is known, the transition state frequencies can be estimated so as to obtain $\Delta S^{\ddagger}$ values of the appropriate sign.

In these studies, the nature of the process was known, so the transition state frequencies were estimated in order to obtain a $\Delta S^{\ddagger}$ value of the appropriate sign and range (typically values are ~12 J mol^{-1} K^{-1} for simple bond dissociation reactions and ~-12 J mol^{-1} K^{-1} for isomerization reactions). The transition states were made loose or tight by scaling the lowest five vibrational frequencies by a common factor (greater than 1.0 to yield a $\Delta S^{\ddagger} < 0$ and less than 1.0 to produce a $\Delta S^{\ddagger} > 0$). The lowest five frequencies were chosen as they contributed most to the calculated sums and densities of states.

References

[1] W. Paul, Angew. Chem 29 (1990) 739.

[2] W. Paul and H. Steinwedel *Apparatus for separating charged particles of different specific charges.* German Patent 944,900, 1953; U. S. Patent 2,939,952, 7 June 1960.

[3] R. E. March and R. J. Hughes, Quadrupole Storage Mass Spectrometry,Wiley Interscience, New York, 1989.

[4] R. E. March, J. Mass Spectrom. 32 (1997) 351-369.

[5] R. E. March and J. F. J. Todd *Practical Aspects of Ion Trap Mass Spectrometry,* CRC Press, Boca Raton, 1995.

[6] G. C. Stafford, P. E. Kelley, J. E. P. Syka, W. E. Reynolds and J. F. J. Todd, Int. J. Mass Spectrom. Ion Processes 60 (1984) 85.

[7] R. D. Knight, Int. J. Mass Spectrom. Ion Processes 106 (1991) 63.

[8] E. Mathieu, J. Math. Pure Appl. 13 (1868) 137.

[9] M. Meot-Ner, in Gas-Phase Ion Chemistry, M. T. Bowers (Ed), Academic Press, New York, 1979.

[10] P. Langevin, Ann. Chem. Phys 5 (1905) 245.

[11] T. Su and W. J. Chesnavich, J. Chem. Phys. 76 (1982) 5183-5185.

[12] T. F. Moran and W. H. Hamill, J. Chem. Phys 39 (1963) 1413-1422.

[13] W. J. Chesnavich, T. Su and M. T. Bowers, J. Chem. Phys. 72 (1980) 2641-2655.

[14] T. Su and M. T. Bowers, J. Chem. Phys. 58 (1973) 3027-3037.

[15] T. Baer and P. M. Mayer, J. Am. Soc. Mass Spectrom. 8 (1997) 103-115.

[16] T. Beyer and D. R. Swinehart, ACM Commun. 16 (1973) 379.

[17] T. Baer and W. L. Hase, Unimolecular Reaction Dynamics, Theory and Experiments, Oxford University Press, New York, 1996.

Chapter 3

Experimental Procedures

3.1 Introduction

In this chapter, the components of the ion trap mass spectrometer employed to conduct the work presented in this thesis will be described, in addition to citing all experimental procedures undertaken. The instrument used for all studies was a Finnigan GCQ™ ion trap mass spectrometer, which was operated using the Xcaliber™ software package.

3.2 Instrument

The instrument consists of two components which include a gas chromatograph (GC) interfaced to a quadrupole ion trap. The components and ion optics of the Finnigan GCQ™ ion trap mass spectrometer have been published by the manufacturer [1] but the instrument at the University of Ottawa has undergone some modifications over the past two years and hence, it will be described in detail in this chapter. A general schematic diagram of the mass spectrometer portion of the instrument is shown in Figure 3.2.1.

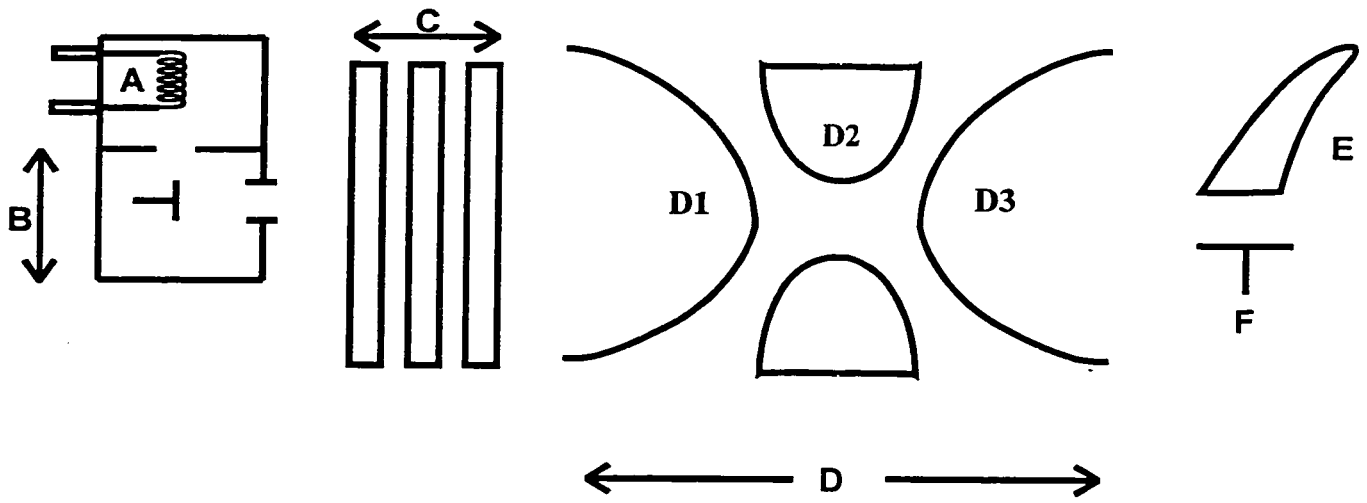

Fig. 3.2.1 Schematic of the Finnigan GCQ™ Ion Trap Mass Spectrometer; A. Filament, B. Ion Volume, C. Einzel Lens Assembly, D. Ion Trap, E. Electron Multiplier, F. Conversion Dynode

3.2.1. Ion Source of the Finnigan GCQ™ ion trap

The ion source is the part of the mass spectrometer where the ions to be studied are made. The GCQ uses an interchangeable ion volume (B) in the source so that two different ionization modes can be used. The interchangeable ion volumes are known as electron ionization and chemical ionization ion volumes and in this work, the "chemical ionization" ion volume was used. This type of ion volume consists of an enclosed volume with small holes to permit sample and electron beam introduction and ion extraction. It is used to achieve higher sample pressures, which increases the probability of auto-protonation of sample molecules.

Liquid sample is introduced through a GC injection septum into a stainless steel reservoir (located inside a GC oven) held at 180 °C where it is volatilized. The vapour is bled into the ion source of the GCQ via a fused-silica capillary of 0.25 mm i.d.

Once inside the ionization chamber, the gaseous sample molecules are exposed to an electron beam emanating from the filament (A) and are ionized. The filament consists of a small loop of rhenium wire through which is passed approximately 1.0 amp of current to produce electrons from thermionic emission. The electrons emitted by the filament are then repelled away from the filament toward the ion volume by the reflector, which is held at a positive potential with respect to the source block (usually +50V to +100V). Both the filament and its reflector are kept at a negative potential relative to the ionization chamber. The electrons emitted by the filament are therefore accelerated and enter the ionization chamber via a small hole. It is these

energetic electrons which ionize the sample molecules.

Some electrons travel across the ionization chamber to the electron trap, positive with respect to the source block, where the current produced can be monitored. Two permanent magnets at opposite ends of the source, parallel to the path of the electrons, collimate the electrons into a beam and provide sufficient magnetic field to cause the electron to take a spiral path through the ionization chamber, increasing the time they spend there and thus increasing the chance that a molecule/electron encounter will occur. This ensures optimum ionization of the sample.

In between the filament and ion volume lies the electron lens. It serves to prevent positive ions from travelling up the electron beam. The voltage applied to it affects the flux of electrons that enter the ion volume; as such, the electron lens voltage can be used to terminate ionization and to control ionization efficiency.

Any unionized species present are eventually lost to the differential pumping system, which consists of an oil diffusion pump backed by a rotary pump. Anions produced by electron capture are accelerated into the base of the ion source by the positive potential difference applied to the entire source assembly. Cations formed are pushed out of the ionization chamber by the repeller electrode which is typically positive with respect to the ion source block by a few volts.

3.2.2 Einzel Lens Assembly

The GCQ contains an einzel-style lense assembly, composed of three lenses (C), which pass and focus ions created in the ion source into the ion trap mass analyser. The lenses consist of stainless steel plates with one or more holes and tubes to which voltages are applied. The lenses can be used to accelerate or decelerate ions as the ions approach the lenses as well as focus an ion beam as the beam passes through the lenses. Both the source block and ion volume are maintained at ground potential with respect to the lens. The potentials applied to the lenses are adjusted during the automatic tune procedure to maximize the flow of ions into the mass analyser.

Lenses 1 and 3 are set to similar potentials (-25V) while the central lens is set to a potential considerably higher than the other two (-100V). The central lens, otherwise known as a gate lens, acts as an ion gate to control the flow of ions to the ion trap mass analyser. It does this by switching polarity between the ion injection and storage phase and the scan out phase of mass analysis. During ion injection and storage phase, the gate lens is held at a polarity to attract ions out of the ion volume and pass them into the ion trap (-100V). During the scan out phase, the polarity is switched to repel additional ions back toward the ion volume (i.e. lens closed) so that they do not interfere with the trapped ions (+100V).

3.2.3 Ion Trap

The mass analyzer, also called the quadrupole ion trap, is the site of ion storage and mass analysis. It consists of three stainless steel electrodes: an entrance end-cap electrode (D1), a central ring electrode (D2) and an exit end-cap electrode (D3). In the GCQ, these three electrodes are separated by silicon nitride spacers. The inner surfaces of the electrodes are hyperbolic in geometry and together, they form a cavity in which ion storage and mass analysis occur.

Both end-cap electrodes have a single small hole in their centers to permit the passage of ions into and out of the mass analyzer cavity. Ions and helium buffer gas enter the mass analyzer cavity through the entrance end-cap electrode. During mass analysis, ions can be ejected through either end-cap electrode; however, it is only those ions ejected through the exit end-cap electrode which are focussed by the exit lens (at ground potential) towards the ion detection system (i.e., conversion dynode/electron multiplier assembly) and detected.

When the proper RF voltage is applied to the central ring electrode relative to both end-cap electrodes, a three dimensional rotationally symmetric quadrupole electric field is created. Ions of selected m/z ratios can be stored in this field in stable orbits. As the RF voltage is increased, the trajectories of the ions become unstable in order of increasing m/z ratios. Ions with unstable orbits are ejected from the ion trap mass analyzer and passed onto the ion detection system (see section 2.2).

3.2.4 Ion Detection System

The GCQ MS detector includes a continuous-dynode electron multiplier (E) and a 15 kV conversion dynode (F); both components are located behind the mass analyzer.

The conversion dynode is a concave metal surface that is located at a right angle to the ion beam; a potential of -15 kV is applied to the conversion dynode for positive ion detection. When an ion strikes the surface of the conversion dynode, one or more secondary particles are produced. These secondary particles are focussed by the curved surface of the conversion dynode and accelerated by a voltage gradient into the electron multiplier.

The electron multiplier is mounted on the top cover plate of the vacuum manifold next to the mass analyzer. The electron multiplier includes a cathode and an anode. The cathode of the electron multiplier consists of a lead-oxide, funnel-like resistor, that holds a potential of up to -3 kV. The exit end of the cathode (at the anode) is near ground potential. The anode of the electron multiplier is a cup located at the exit end of the cathode and collects the electrons produced by the cathode.

Secondary ions, usually electrons, from the conversion dynode strike the inner walls of the electron multiplier cathode with sufficient energy to eject electrons. The ejected electrons are accelerated farther into the cathode, drawn by the increasingly positive potential gradient. Due to the funnel shape of the cathode, the ejected electrons do not travel far before they again

strike the inner surface of the cathode, thereby causing the emission of more electrons. Thus, a cascade of electrons is created that finally results in a measurable current at the end of the cathode where the electrons are collected by the anode. The current collected by the anode is proportional to the number of secondary particles striking the cathode.

Typically, the electron multiplier has a gain of about 10^5 (i.e., for each ion or electron that goes in, 10^5 electrons go out). If the current of ions and electrons entering the electron multiplier from the conversion dynode is 10^{-12} A and the gain of the electron multiplier is 10^5, then a current of 10^{-7} A leaves the electron multiplier via the anode. This current is converted to a voltage by the electrometer circuit and recorded by the data system.

3.3 Procedure

All data was acquired through the use of a program entitled GCQ Tune and all steps to the acquisition of a mass spectrum are cited in Appendix 1.

Samples (highest purity available) were purchased from Sigma-Aldrich Fine chemicals. The vapour of sample volatilized in the reservoir was bled into the ion source of the GCQ via a fused-silica capillary of 0.25 mm i.d. Neutral reagent sample vapour, on the other hand, was introduced into the vacuum chamber via a Granville-Phillips™ variable leak valve at ambient temperature. Samples injected into the GCQ portion of the instrument were used without further purification, while the neutral reagent used was degassed by several freeze-pump-thaw cycles

prior to use to remove any existing impurities (i.e. air, volatiles) from the reagent. This involves freezing the reagent in a dewar flask, pumping the reagent down to about 45 mTorr and then allowing it to thaw. Reagent pressure was monitored with a Bayert-Alpert type ionization gauge.

Protonated molecules were generated in the chemical ionization ion source of the GCQ by self protonation after ionization by 70 eV electrons. Ion/molecule reactions in the ion source eventually produce protonated molecules AH^+ (see example below).

e.g.
$$CH_3CN \rightarrow CH_3CN^{+\cdot}$$
$$CH_3CN^{+\cdot} + CH_3CN \rightarrow \dot{C}H_2CN + CH_3CNH^+$$

All ions generated by electron impact were gated into the ion trap by applying a focussing potential to the central lens in the einzel lens assembly. Ion/molecule reactions were studied in the MS^2 mode of the GCQ. This involves isolating an ion with the m/z value of interest by applying a broad-band RF field to the end-cap electrodes (which resonantly excites all ions in the trap), out of which was notched a frequency corresponding to the ion of interest. An isolation time of 2 ms was used, although longer times were tried and found to have no effect on the final rate constant.

Following isolation, the trapping mode was changed to store, for a variable length of time (between 1 and 30 ms), all product ions of the reaction between the isolated reactant ion and neutral reagent present in the trap. The mass spectrum for a given reaction time was acquired by sequentially scanning ions out of the trap where they were detected with the conversion

dynode/electron multiplier assembly. Each experiment was performed an average of six times and all errors are based upon these measurements. The reaction time window and pressure regime that can be studied with the current instrument configuration limits observations to rate constants between 10^{-12} and 10^{-9} cm^3 $molecule^{-1}$ s^{-1}.

3.4 Calibration Reaction

When determining the absolute pressure of neutral reagent in the ion trap, two factors must be taken into consideration: the ionization gauge response to that particular molecule and the relative pressures of the reagent in the vacuum chamber and inside the trapping volume. A correction for both these effects was obtained by measuring the rate constant for the well-studied reaction between acetone and the acetyl cation [2,3]:

$$\underset{\text{m/z 43}}{(CH_3)_2C{=}O + CH_3CO^+} \rightarrow \underset{\text{m/z 59}}{(CH_3)_2C{=}OH^+} + CH_2CO$$

The resulting spectra contained two peaks, m/z 43 and m/z 59. Experiments were performed at a series of different acetone pressures whereby the reaction times were varied from 1 - 30 ms (Fig. 3.4.1). The peak heights for the m/z 43 (H_{43}) and m/z 59 (H_{59}) ions were measured and a plot of ln $[H_{43}/(H_{43}+H_{59})]$ vs. reaction time was made for each pressure; the slope of each plot yielding a pseudo-first order rate constant (Fig. 3.4.2). A plot of the pseudo-first order rate constant as a function of acetone pressure yields the bimolecular rate constant for the reaction

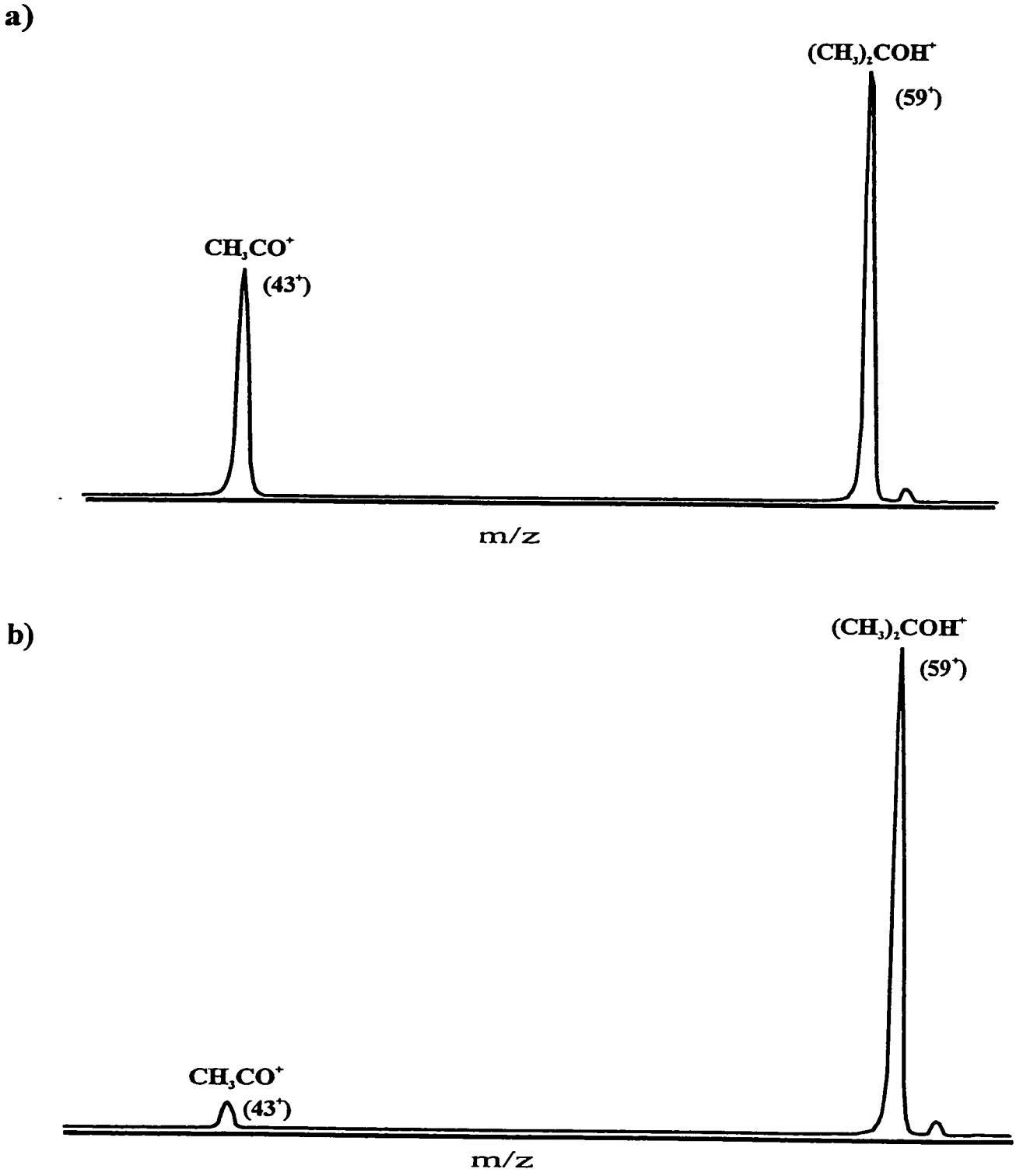

Fig. 3.4.1 Mass spectra corresponding to reaction times a) 1 ms and b) 30 ms for the ion/molecule reaction between CH_3CO^+ and acetone.

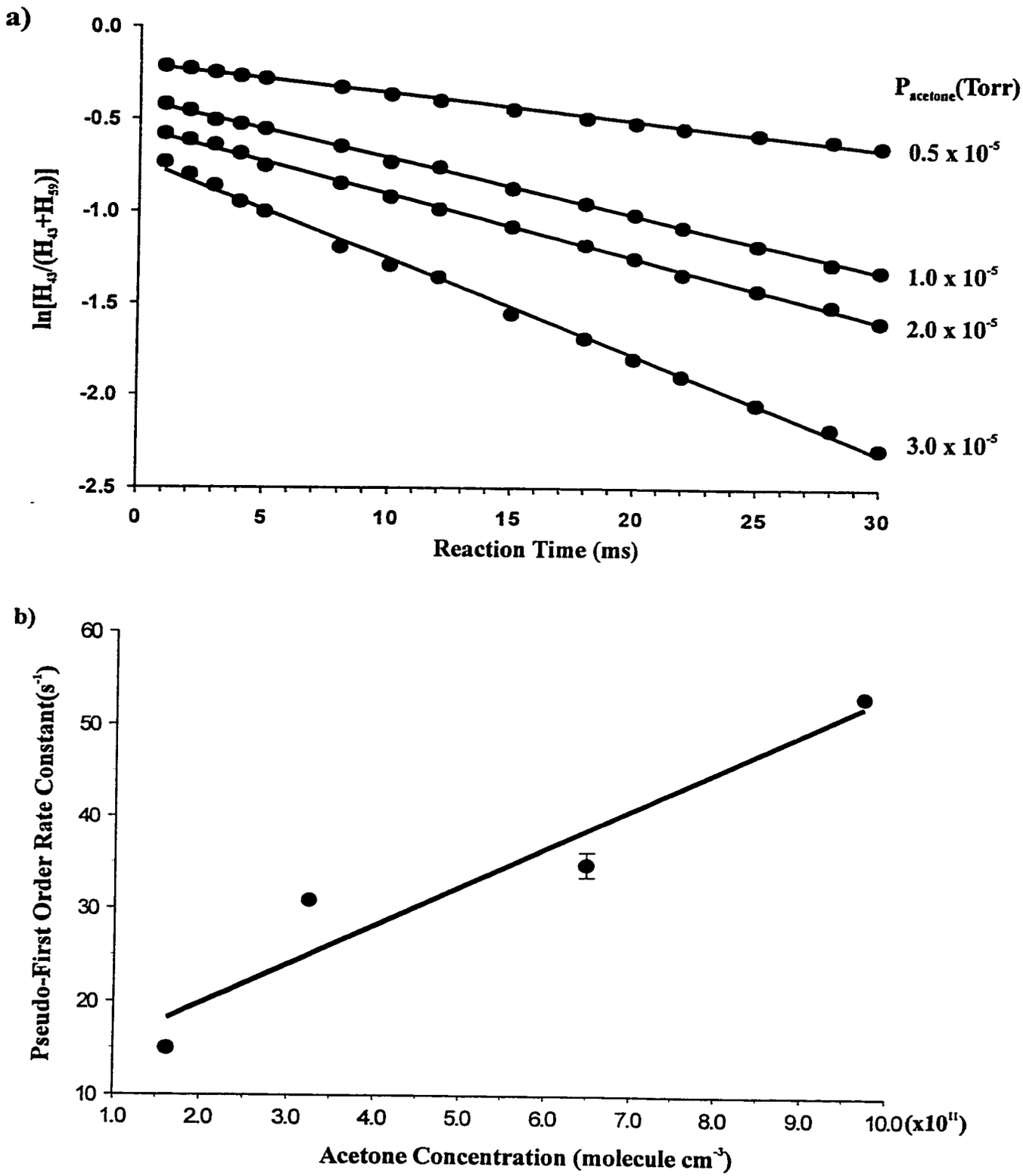

Fig. 3.4.2 a) Pseudo-first order plots for the reaction: $(CH_3)_2C{=}O + CH_3CO^+ \rightarrow (CH_3)_2COH^+ + CH_2CO$ at four neutral acetone pressures (laboratory frame of reference). b) Plot of the pseudo-first order rate constant as a function of acetone pressure. Acetone pressures were corrected as outlined in the text to achieve a bimolecular rate constant of 2.1×10^{-10} cm^3 molecule^{-1} s^{-1}.

(Fig. 3.4.2). This experimentally derived value was then corrected to the literature value of 2.1 x 10^{-10} cm^3 $molecule^{-1}$ s^{-1} [2] resulting in a correction factor of 0.16 (± 0.03) for the neutral acetone pressure in the ion trap volume. This calibration was performed numerous times over the course of the study, and the resulting correction factor did not change significantly. When neutrals other than acetone were used, an additional correction was applied to account for the different response of the ionization gauge between that neutral and acetone [4].

3.5 Temperature of the Reaction

One question that arises is the temperature of ions in the ion trap. The presence of helium buffer gas should assist in the thermal equilibrium of ions generated in the "hot" ion source of the instrument provided they are stored for sufficient time. To explore this further in our system, the effect of helium gas pressure on the final bimolecular rate constant was determined. Typically, the pressure of helium within the trap is ca. 1 mTorr, but the pressure measured in the vacuum chamber by the ionization gauge is ca. 1.0 x 10^{-5} Torr. To assess the impact of He pressure on the measured ion/molecule rate constant, the pressure of He was increased so that the chamber pressure was 1.2 x 10^{-5} Torr and 2.4 x 10^{-5} Torr. No change in rate constant was measured for the calibration reaction at these different He pressures, indicating that ions injected into the trap are likely thermalized to ambient temperature. In addition, since the ion trap electrodes are not heated (the instrument incorporates an external ion source), the temperature within the trap is estimated to be 298 K.

Appendix 1. The Acquisition of a Mass Spectrum

1. Select the GCQ Tune icon. This will load the page required to operate the ion trap.

2. Select ON. This will activate the filament and multiplier to allow for ions to be produced.

3. Select Instrument/ Ionization Gauge. This will indicate the pressure within the ion trap.

4. Select Experiment/Full Scan. This will allow the full spectrum of all the ions present in the trap to be revealed. This provides the option of specifying what mass range to study. For these studies, the mass range was from 25- 125 amu.

5. For the ion/molecule reactions, select Experiment /MS^n. It is within this window that the reaction parameters are specified. This window (Fig. 3.5.1) is subdivided into two sections: isolation and excitation. The precursor ion (i.e., the ion component of the ion/molecule reaction) is selected and isolated for a set period of time prior to reacting with any neutrals present in the trap. In these studies, the isolation time was held constant at 2 ms, while the reaction (excitation) time was varied from 1 to 30 ms over the course of the experiment. It is the variability of this parameter that allows a rate constant to be determined. The isolation width (i.e., the width of the window around the m/z ion of interest isolated during MS/MS experiments) was always set at 1.2, while the excitation voltage was always set at zero. This is because ion/molecule reactions are exothermic in nature and thus, require no additional internal energy. The excitation

"q" (i.e., q_z) was always set at 0.225 as it was found to be the most appropriate for these studies.

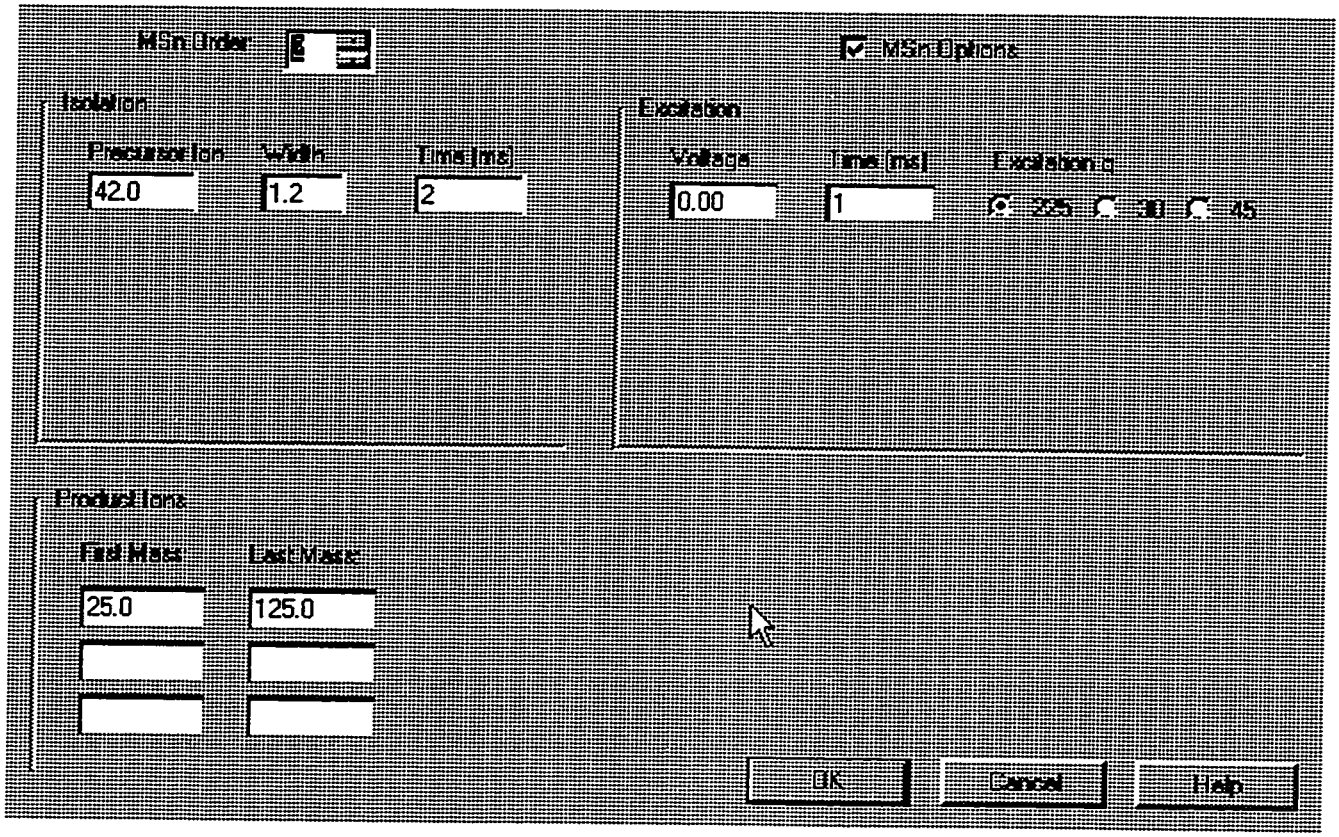

Fig 3.5.1 Window used to study ion/molecule reactions on the Finnigan GCQ Ion Trap Mass Spectrometer.

References

[1] R. Heather, MS Detector Operator's Manual Editor, Technical Publications, Finnigan MAT, San Jose,1995.

[2] R. Carpignano, L. Operti, R. Rabezzana and G. A. Vagglio, J. Am. Soc. Mass Spectrom. (1998) 938-944.

[3] R. Grover, M. Decouzon, P.-C. Maria and J.-F. Gal, Eur. Mass Spectrom. 2 (1996) 213-223.

[4] J. E. Bartmess and R. M. Georgiadis, Vacuum 33 (1983) 149-153.

Chapter 4

The Energetics of the Dehydration of Proton-Bound Alcohol Dimers

4.1 Introduction

Clusters of molecules are often viewed as an intermediate state of matter between the dilute gas phase and solution. Studying clusters allows the effects of solvation on the chemistry of gas-phase molecules and ions to be explored [1-5]. Ionic clusters (typically made up of a core ion surrounded by one or more solvating molecules) are known to be involved in the chemistry of the upper and mid atmosphere [6]. A central issue, when studying the chemistry of all gaseous ions, is their propensity for rearrangement prior to reaction. Over the years, a variety of thermodynamically stable structures have been discovered and found to be involved in ion dissociation mechanisms, including distonic ions [7], ion-neutral complexes [8,9] and bridged ions [10]. The isomerization of organic ions is well known, and appears to be a common occurrence [11-15]. The isomerization of cluster ions, in addition to being a scientific curiosity, can also have an impact on the kinetics of the reactions between ions and molecules in the gas phase. Even though there may not be an activation barrier to an ion/molecule reaction, the presence of the isomerization on the reaction surface can make the reaction less efficient. Computational chemistry has made it possible to characterize isomerization pathways. However, as the ions under investigation get larger, it becomes increasingly more computationally intensive to reliably identify transition structures and intermediate equilibrium species on potential energy surfaces. Therefore, it is valuable to be able to experimentally estimate the net isomerization

barrier height in a reaction, even though the exact mechanism for the process may not be known.

In the present study, the formation of products due to the isomerization of proton-bound alcohol dimers is of interest. The family of proton-bound alcohol dimers all have at least one common feature; they exhibit in their unimolecular chemistry the competition between simple bond dissociations and dehydration reactions. Calculations [16-18] and experiments [19-29] on the methanol dimer ion indicate that isomerization proceeds via an internal S_N2 reaction. Essentially, the dehydration reactions consist of a backside nucleophilic attack of a neutral alcohol on the alkyl group of a protonated alcohol, forming in sequence, two stable intermediate complexes, $[RO(H)\bullet\bullet\bullet R'\text{-}OH_2]^+$ and $[RO(H)\text{-}R'\bullet\bullet\bullet OH_2]^+$. The latter can then rearrange to the proton-bound dimer $(RR'O)(H_2O)H^+$ prior to water loss [16-18].

These systems can also be approached from the point of view of an ion/molecule reaction. When an ion and molecule react in the gas-phase, there are several basic processes that can occur, as shown below.

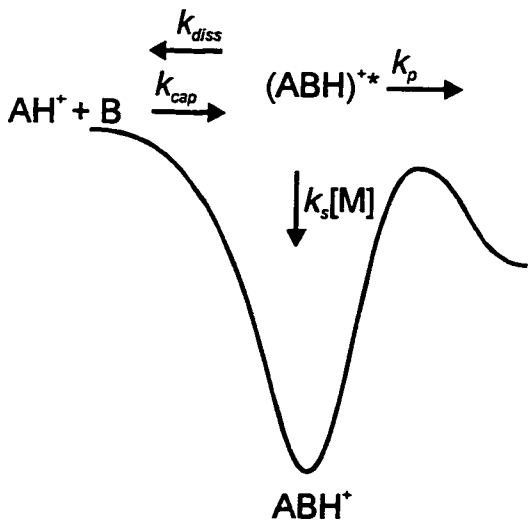

Initially, AH^+ and B must form an excited dimer ion, $(ABH^+)^*$. The rate constant for this process is denoted by k_{cap}. Once formed, $(ABH^+)^*$ can dissociate, k_{diss}, or be stabilized by collision with a third body, M, to form stable dimer ions, ABH^+, (k_s[M]). The dimer can also react further to form products and the rate constant for

this process is denoted as k_p. Both the dissociation and isomerization channels shown previously are unimolecular processes while the third body collision, k_s[M], is a bimolecular reaction. The radiative stabilization of the complex (i.e., stabilization of $(ABH^+)^*$ by emission of an infrared photon) has been ignored here due to its long timescale.

The reactions involving protonated and neutral alcohols can be written as follows:

$$R_1OH_2^+ + R_2OH \rightarrow (R_1)(R_2)OH^+ + H_2O \qquad (4.1.5)$$

The rate constant, k_{obs}, for the formation of protonated ether and water can be written as [30]:

$$k_{obs} = \rho_{cap} k_{cap} \left(\frac{k_p}{k_p + k_{diss} + k_s[M]} \right) \qquad (4.1.6)$$

The probability that a collision will lead to a long-lived excited intermediate complex is denoted ρ_{cap}. The association reaction can normally be assumed to occur on every collision (i.e., $\rho_{cap} = 1$), though care must be taken when making this assumption [31]. The rate constant for capture collisions occurring between the reactant ion and neutral, k_{cap}, can be calculated using the ion-dipole theory of Su and Chesnavich [32], while k_s[M] (the rate constant for collisional stabilization of the initially formed excited complex) is typically derived from the ion-induced dipole theory developed by Langevin [33]. In these systems, k_p most directly reflects the rate constant for the isomerization of the initially formed proton-bound dimer, k_{iso}, which ultimately leads to water loss. Since k_{iso} can be modelled using RRKM theory [34], information that can be obtained about it can yield the energetics of the isomerization of the dimer.

4.2 Results and Discussion

The experimental results are summarized in Table 4.2.1.

4.2.1 Reactions not displaying a proton-bound dimer ion

The reaction between protonated and neutral methanol,

$$\underset{m/z\ 33}{CH_3OH_2^+} + CH_3OH \rightarrow \underset{m/z\ 47}{(CH_3)_2OH^+} + H_2O \qquad (4.2.1)$$

was studied and two peaks were observed in the mass spectrum: m/z 33 ($CH_3OH_2^+$) and m/z 47 (Fig. 4.2.1). The latter is known to be protonated dimethylether, $(CH_3)_2OH^+$, and is observed as a unimolecular dissociation product of proton-bound methanol dimer ions [16,19,20,22,25-27,38]. The peak heights of the m/z 33 (H_{33}) and m/z 47 (H_{47}) ions were measured and a first-order plot of ion intensity, $[\ln(H_{33}/(H_{33} + H_{47})]$, vs. reaction time yielded pseudo-first order rate constants (Fig 4.2.2(a)). These rate constants were then plotted against their respective methanol pressures to yield the bimolecular rate constant for the reaction. The line in Fig. 4.2.2(b), similarly to the lines present in all other bimolecular plots, is from a least squares regression. The correction factor obtained from the acetone calibration experiment was applied to the methanol pressures (plus a correction for the different ion gauge response between acetone and methanol [27]) to obtain the corrected experimental bimolecular rate constant of $(1.1 \pm 0.1) \times 10^{-10}$ cm^3 molecule^{-1} s^{-1} (Fig.4.2.2(b)). This value compares extremely well with experimental rates derived from ICR techniques. McMahon and Beauchamp [29] derived a

value of 1.1×10^{-10} cm^3 molecule^{-1} s^{-1}, while Karpas and Meot-Ner [19] obtained a value of $(1.08 \pm 0.22) \times 10^{-10}$ cm^3 molecule^{-1} s^{-1}. Bass et al. [24] derived a value of $(0.9 \pm 0.3) \times 10^{-10}$ cm^3 molecule^{-1} s^{-1}, while Morris et al.[28] derived a value of 0.8×10^{-10} cm^3 molecule^{-1} s^{-1}. The value derived with the ion trap lies within the experimental uncertainty of each group; all values lying an order of magnitude less than that obtained using the ion-dipole theory of Su and Chesnavich (2.3×10^{-9} cm^3 molecule^{-1} s^{-1}) [32]. The polarizability and dipole moment of methanol were obtained from the literature [39,40]. The quoted uncertainty is based solely on the experimental data and does not take into account uncertainties in the calibration procedure. Therefore, all uncertainties quoted in this work for k_{obs} should be treated as minimum values.

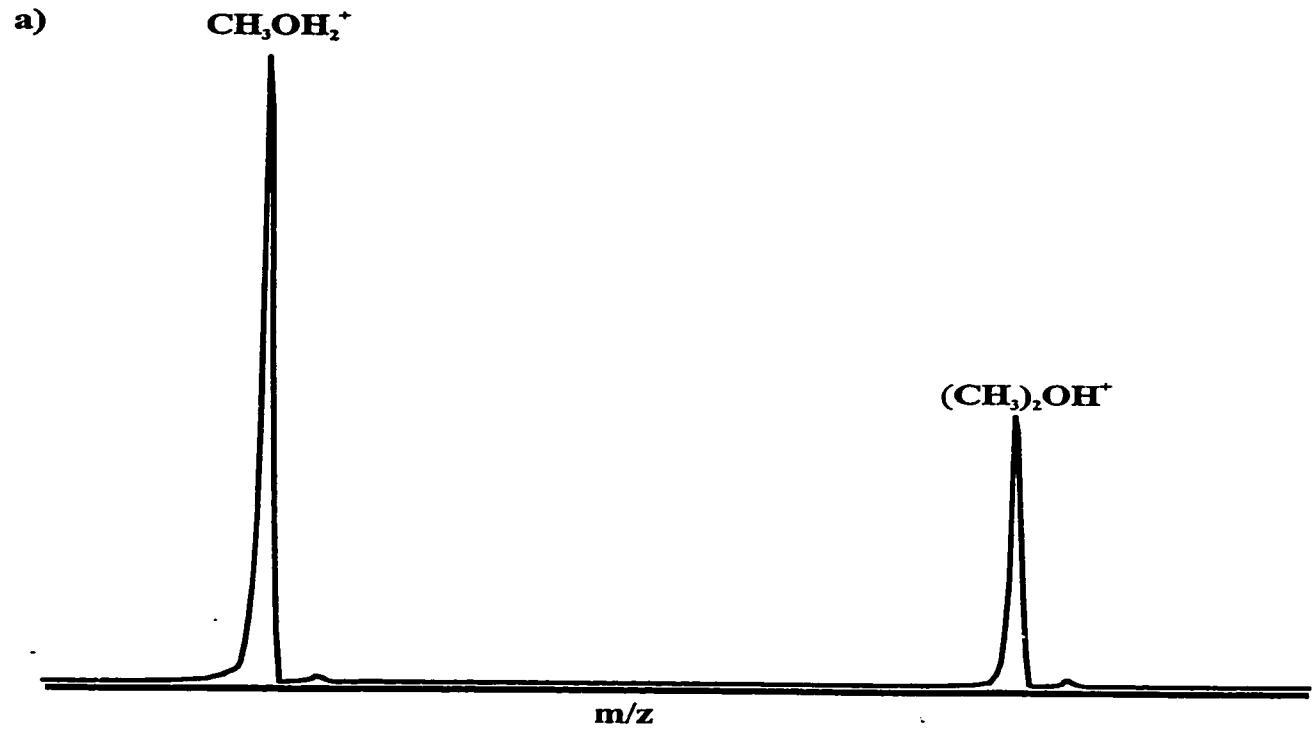

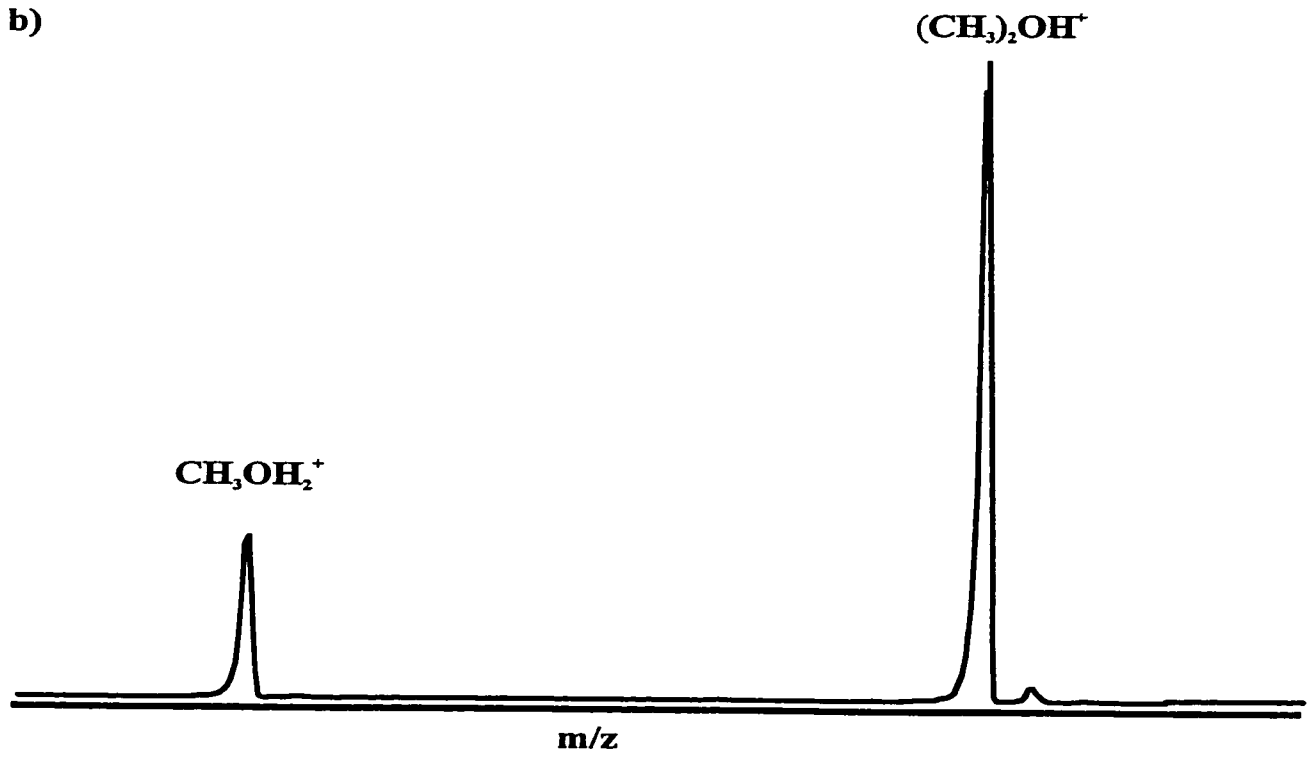

Fig. 4.2.1 Mass Spectra corresponding to reactions times a) 1 ms and b) 30 ms for the ion/molecule reaction between $CH_3OH_2^+$ and CH_3OH.

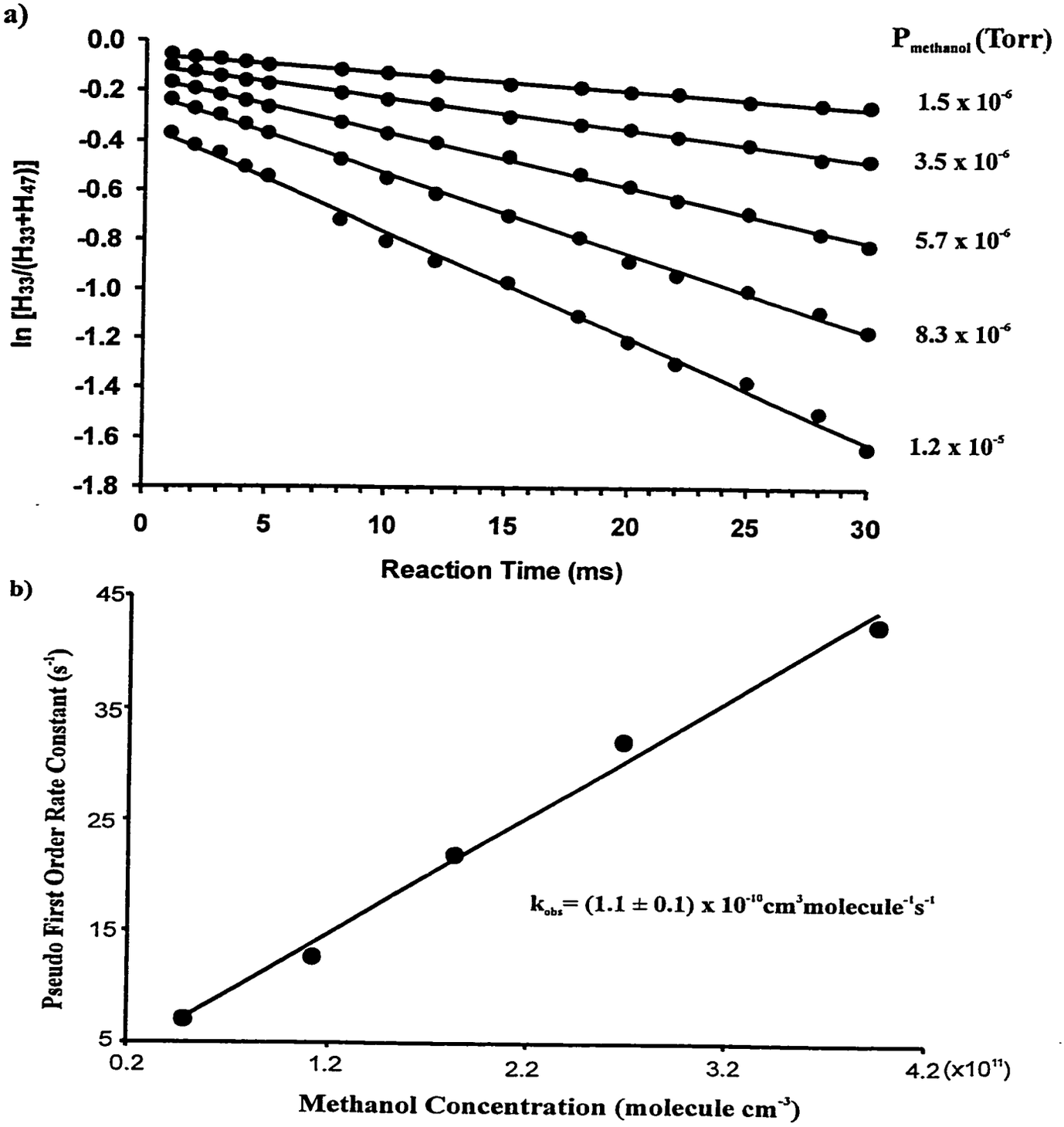

Fig. 4.2.2 a) Pseudo-first order plots for the reaction $CH_3OH_2^+ + CH_3OH \rightarrow (CH_3)_2OH^+ + H_2O$ at five neutral methanol pressures, b) Plot of the pseudo-first order rate constant as a function of methanol pressure. Methanol pressures were corrected as outlined in the text. No error bars were placed on the graph as the experimental uncertainty in the data points was smaller than the points themselves.

4.2.2 Reactions displaying a proton-bound dimer ion

The three systems shown below contained only three ions in their mass spectra, the lowest energy protonated alcohol (A), the proton-bound dimer ion of the two reactants (B) and the protonated ether that is due to the dehydration of this proton-bound dimer ion (C).

$$CH_3CH_2OH_2^+ + CH_3OH \rightarrow (CH_3CH_2)(CH_3)OH^+ + H_2O \quad (4.2.2)$$

$$CH_3CH_2OH_2^+ + CH_3CH_2OH \rightarrow (CH_3CH_2)_2OH^+ + H_2O \quad (4.2.3)$$

$$CH_3CH_2CH_2OH_2^+ + CH_3CH_2OH \rightarrow (CH_3CH_2CH_2)(CH_3CH_2)OH^+ + H_2O \quad (4.2.4)$$

Since the proton-bound dimer is now present in the mass spectra, it must be taken into account when determining the rate constants. As such, plots of ln $[H_A/(H_A+H_B+H_C)]$ were made to obtain the pseudo-first order rate constants. The derived bimolecular rate constants for these three reactions increase in magnitude from $(1.9 \pm 0.5) \times 10^{-11}$ cm^3 molecule^{-1} s^{-1} (Fig. 4.2.3) for reaction (4.2.2) to $(1.4 \pm 0.3) \times 10^{-10}$ cm^3 molecule^{-1} s^{-1} (Fig. 4.2.4) for reaction (4.2.3) and $(2.1 \pm 0.5) \times 10^{-10}$ cm^3 molecule^{-1} s^{-1} (Fig. 4.3.5) for reaction (4.2.4). McMahon and Beauchamp [29] derived a value of 2.4×10^{-10} cm^3 molecule^{-1} s^{-1} for reaction (4.2.3), while Karpas and Meot-Ner [19] derived a value of $(0.68 \pm 0.11) \times 10^{-10}$ cm^3 molecule^{-1} s^{-1}.

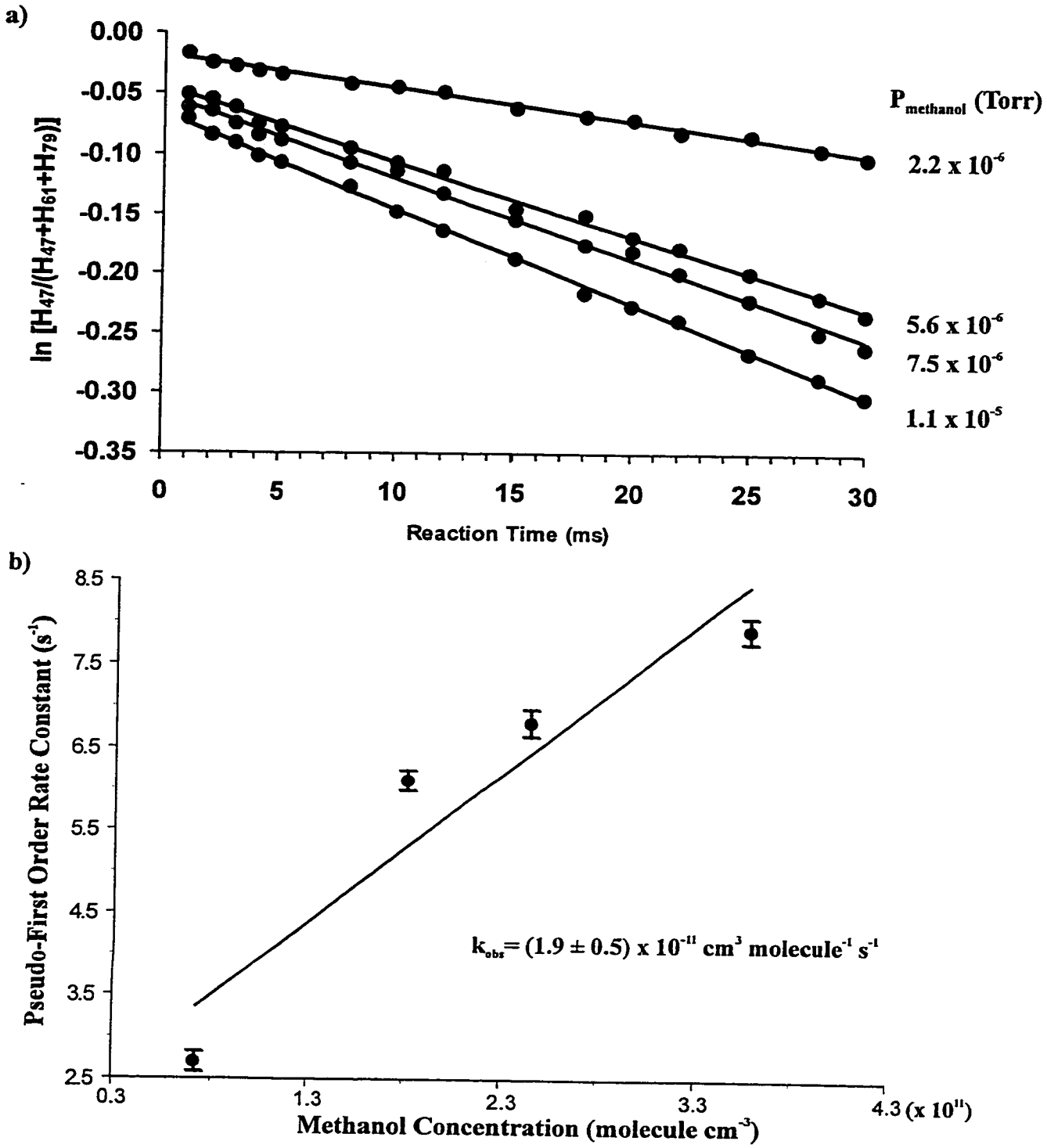

Fig.4.2.3 a) Pseudo-first order plots for the reaction $CH_3CH_2OH_2^+ + CH_3OH \rightarrow (CH_3CH_2)(CH_3)OH^+ + H_2O$ at four neutral methanol pressures, b) Plot of the pseudo-first order rate constant as a function of methanol pressure. Methanol pressures were corrected as outlined in the text.

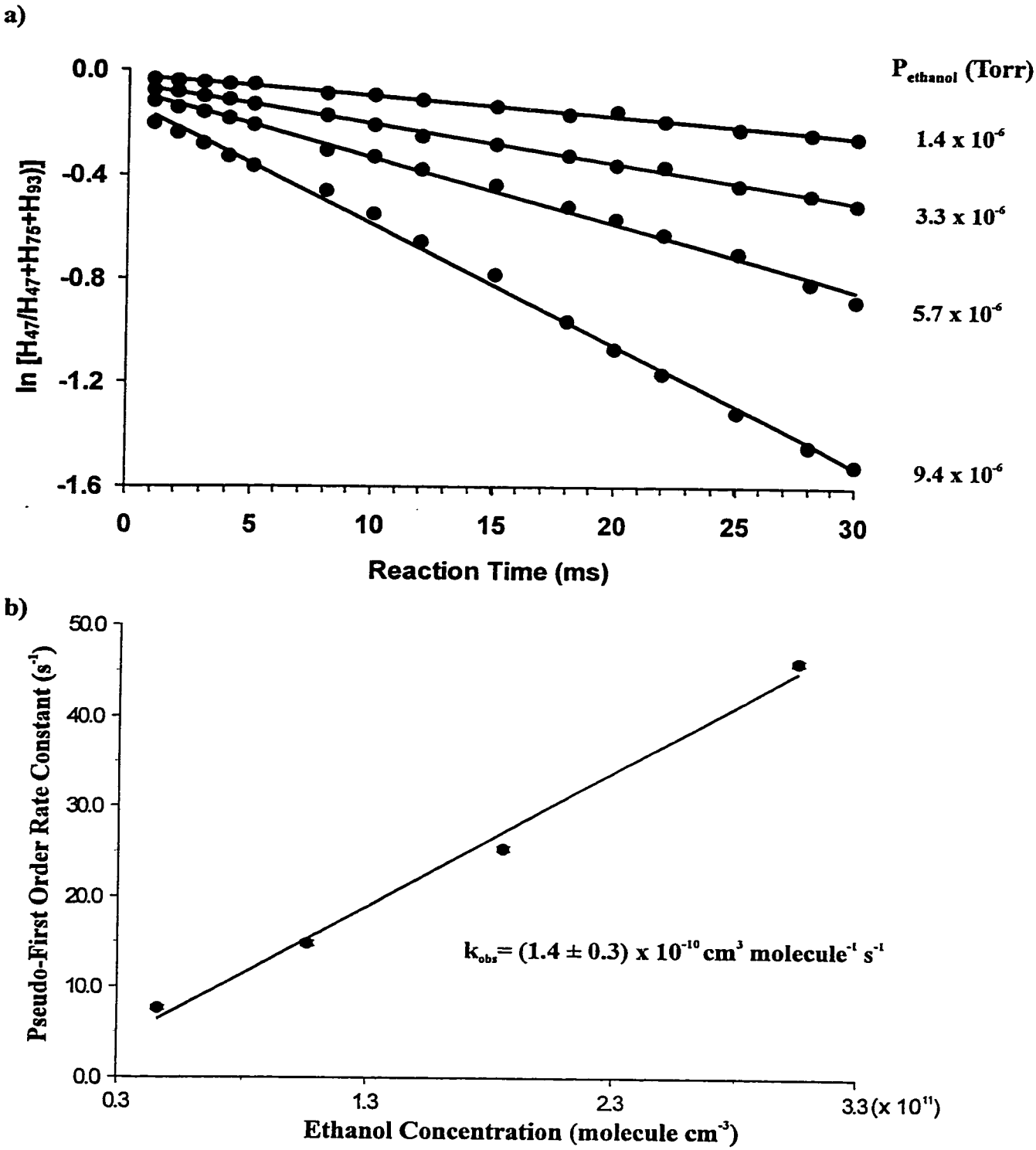

Fig.4.2.4 a) Pseudo-first order plots for the reaction $CH_3CH_2OH_2^+ + CH_3CH_2OH \rightarrow (CH_3CH_2)_2OH^+ + H_2O$ at four neutral ethanol pressures, b) Plot of the pseudo-first order rate constant as a function of ethanol pressure. Ethanol pressures were corrected as outlined in the text.

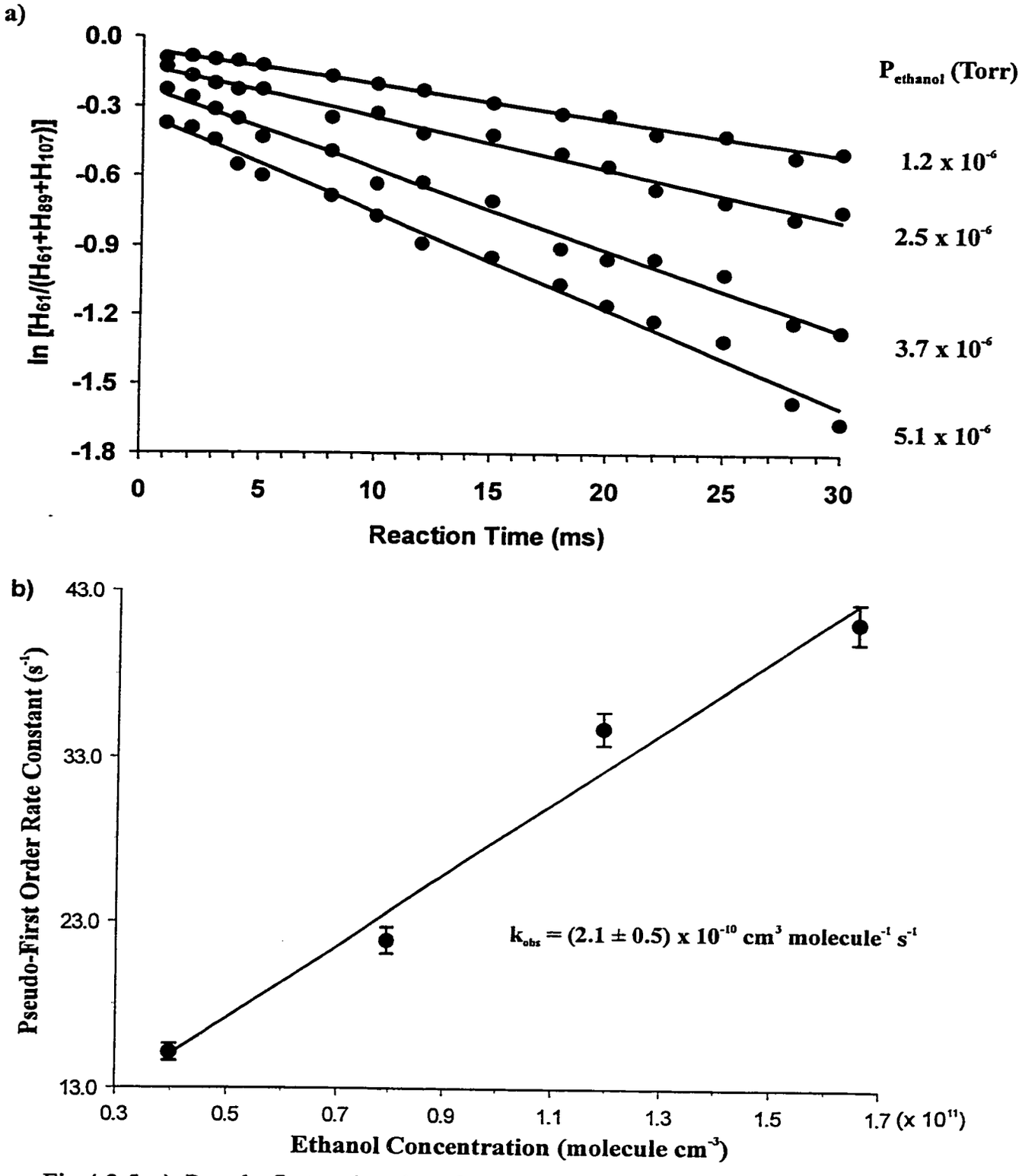

Fig.4.2.5 a) Pseudo-first order plots for the reaction $CH_3CH_2CH_2OH_2^+ + CH_3CH_2OH \rightarrow (CH_3CH_2CH_2)(CH_3CH_2)OH^+ + H_2O$ at four neutral ethanol pressures, b) Plot of the pseudo-first order rate constant as a function of ethanol pressure. Ethanol pressures were corrected as outlined in the text.

4.2.3 Reactions displaying a dimer ion and two product ions

The remaining systems exhibited two reaction products, the protonated ether resulting from dehydration of the dimer ion and a peak due to the loss of an alkene from the dimer ion.

$$CH_3CH_2CH_2OH_2^+ + CH_3OH \rightarrow (CH_3CH_2CH_2)(CH_3)OH^+ + H_2O \rightarrow m/z\ 65 + CH_2{=}CH_2 \quad (4.2.5)$$

$$CH_3CH_2CH_2OH_2^+ + CH_3CH_2CH_2OH \rightarrow (CH_3CH_2CH_2)_2OH^+ + H_2O \rightarrow m/z\ 79 + CH_3CH{=}CH_2 \quad (4.2.6)$$

$$(CH_3)_2CHOH_2^+ + (CH_3)_2CHOH \rightarrow ((CH_3)_2CH)_2OH^+ + H_2O \rightarrow m/z\ 79 + CH_3CH{=}CH_2 \quad (4.2.7)$$

The appearance of the product ion due to alkene loss in the mass spectra of reactions (4.2.5) and (4.2.6) had no appreciable effect on the final bimolecular rate constant as it was a minor process in both cases (less than 3% of the total concentration). As such, its inclusion was not necessary in the final kinetic treatment. It was, however, necessary to include this ion in the treatment of reaction (4.2.7) as it was a significant contribution to the reaction products. The rate constants varied in magnitude from $(6.1 \pm 0.5) \times 10^{-11}$ $cm^3 molecule^{-1} s^{-1}$ for reaction (4.2.5) and $(6.3 \pm 0.3) \times 10^{-10}$ cm^3 $molecule^{-1}$ s^{-1} for reaction (4.2.6) to $(1.1 \pm 0.1) \times 10^{-9}$ $cm^3 molecule^{-1}$ s^{-1} for reaction (4.2.7), a value that is essentially the same as the collision capture rate constant, k_{cap} ($1.9 \times 10^{-9} cm^3 molecule^{-1} s^{-1}$) (Table 4.3.1). Karpas and Meot-Ner [19] obtained values of $(1.03 \pm 0.12) \times 10^{-10}$ cm^3 $molecule^{-1}$ s^{-1} for reaction (4.2.6) and $(6.14 \pm 0.12) \times 10^{-10}$ cm^3 $molecule^{-1}$ s^{-1} for reaction (4.2.7). These values are lower than those obtained with the ion trap.

In the case of reaction (4.2.7), the present k_{obs} reflects the loss of both water and propene, and so will be larger than the rate constant for only water loss. However, the present value will permit the isomerization barrier to be derived as outlined in the following section.

Table 4.2.1

Comparison of the measured ion/molecule reaction rate constants, k_{obs}, with the collision-capture limit, k_{cap}, for the reactions leading to protonated ether and neutral water.

reactants	k_{obs} [a,b]	k_{cap} [a]
$CH_3OH_2^+ + CH_3OH$	0.11 ± 0.01	2.3
$CH_3CH_2OH_2^+ + CH_3OH$	0.019 ± 0.005	2.1
$CH_3CH_2OH_2^+ + CH_3CH_2OH$	0.14 ± 0.03	2.1
$CH_3CH_2CH_2OH_2^+ + CH_3OH$	0.061 ± 0.005	2.0
$CH_3CH_2CH_2OH_2^+ + CH_3CH_2OH$	0.21 ± 0.05	2.3
$CH_3CH_2CH_2OH_2^+ + CH_3CH_2CH_2OH$	0.63 ± 0.03	1.9
$(CH_3)_2CHOH_2^+ + (CH_3)_2CHOH$	1.1 ± 0.1	1.9

[a] In units of 10^{-9} cm^3 $molecule^{-1}$ s^{-1}.

[b] Uncertainties should be viewed as minimum values (see text).

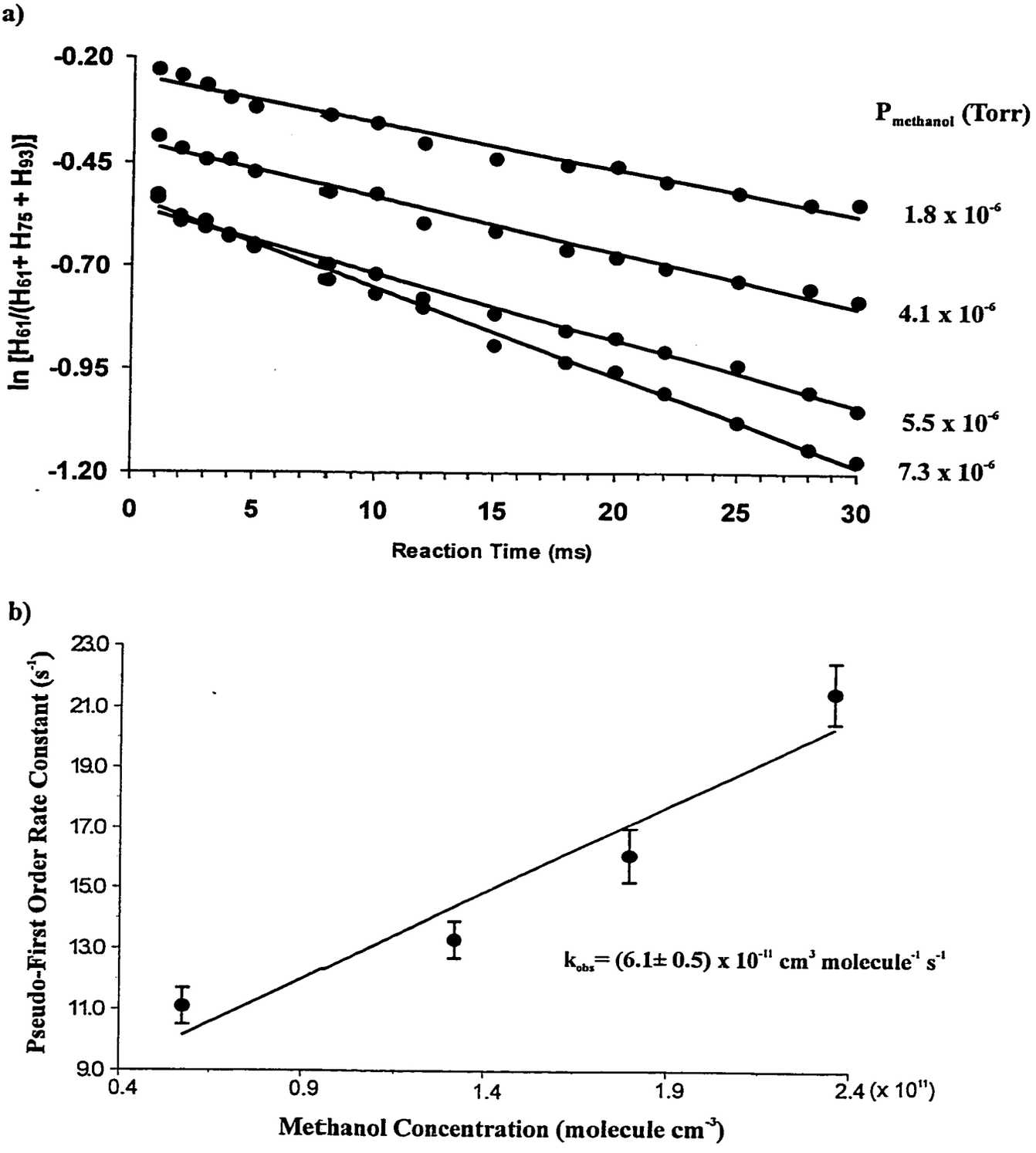

Fig.4.2.6 a) Pseudo-first order plots for the reaction $CH_3CH_2CH_2OH_2^+ + CH_3OH \rightarrow (CH_3CH_2CH_2)(CH_3)OH^+ + H_2O$ at four neutral methanol pressures, b) Plot of the pseudo-first order rate constant as a function of methanol pressure. Methanol pressures were corrected as outlined in the text.

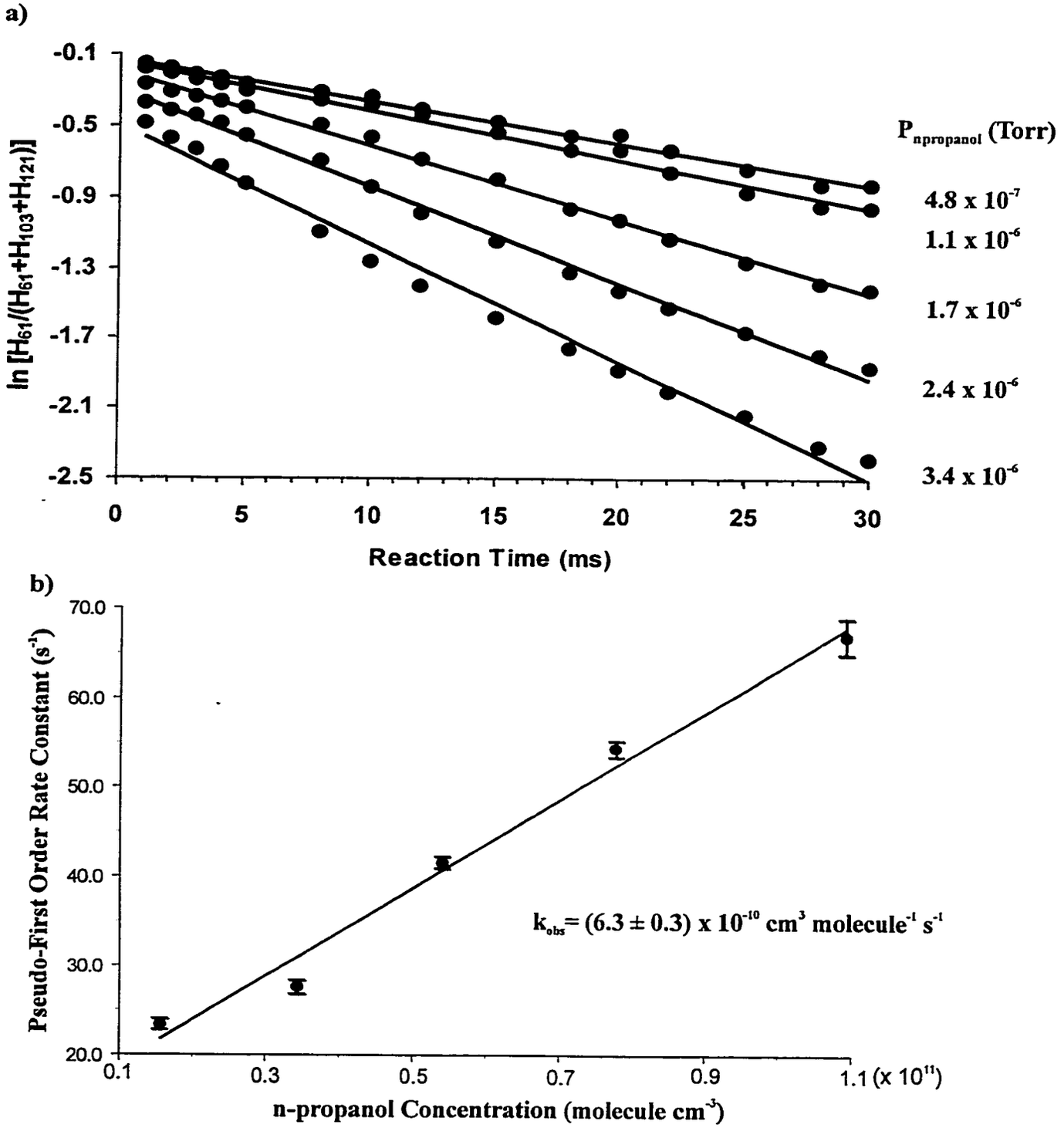

Fig.4.2.7 a) Pseudo-first order plots for the reaction $CH_3CH_2CH_2OH_2^+ + CH_3CH_2CH_2OH \rightarrow (CH_3CH_2CH_2)(CH_3CH_2CH_2)OH^+ + H_2O$ at five neutral n-propanol pressures, b) Plot of the pseudo-first order rate constant as a function of n-propanol pressure.

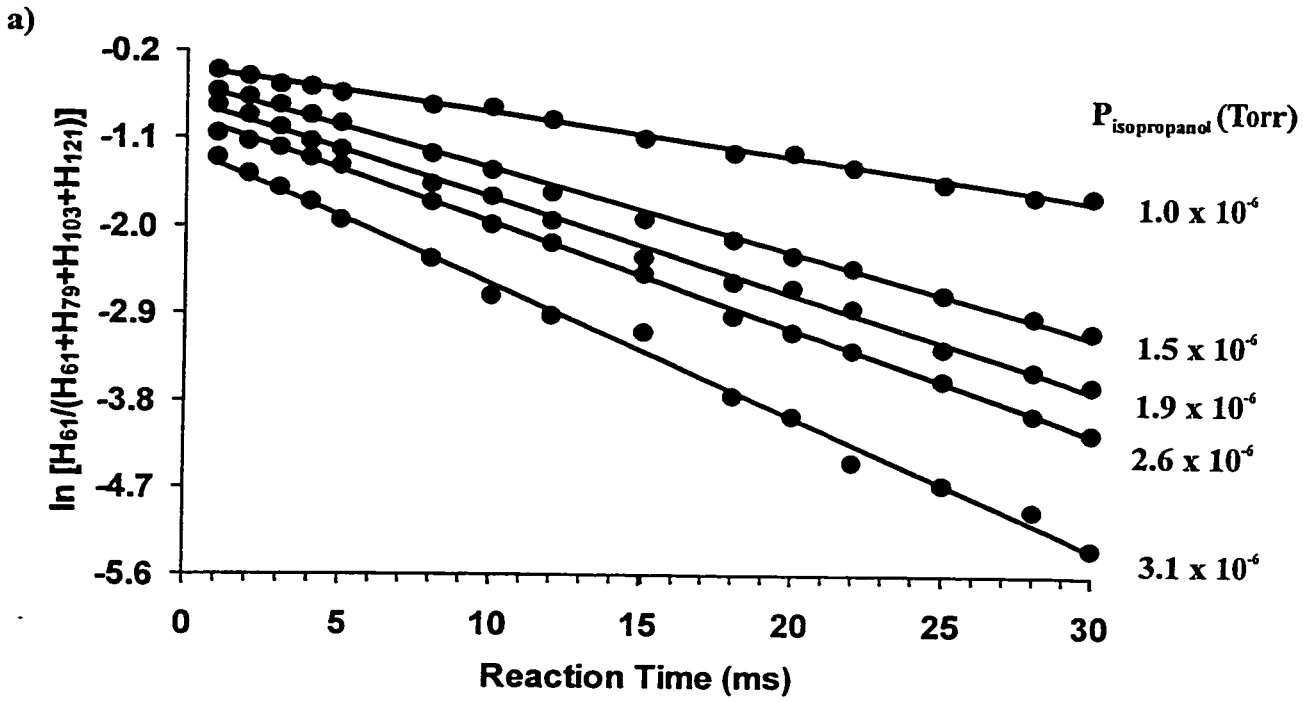

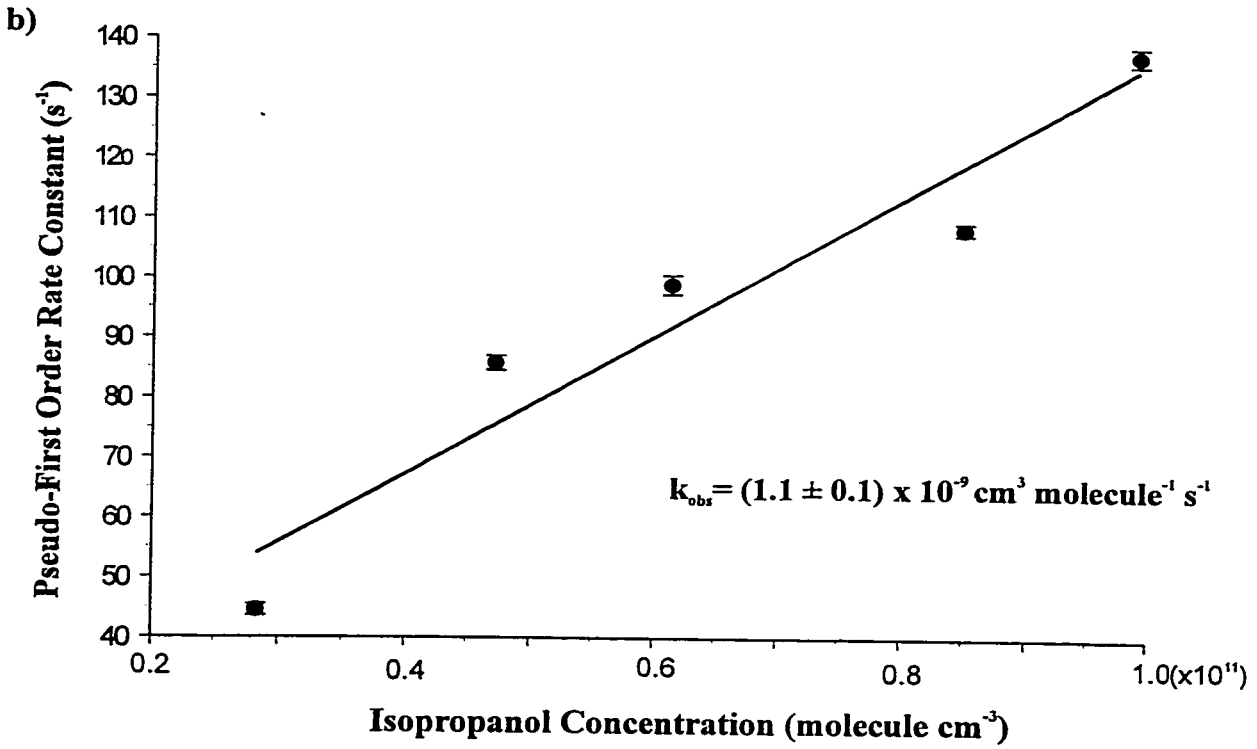

Fig.4.2.8 a) Pseudo-first order plots for the reaction $(CH_3)_2CHOH_2^+ + (CH_3)_2CHOH \rightarrow ((CH_3)_2CH)_2OH^+ + H_2O$ at five neutral i-propanol pressures, b) Plot of the pseudo-first order rate constant as a function of i-propanol pressure.

4.3 Isomerization energy barrier

The rate constants determined above can be used to obtain information about the reaction surface. The ratio of k_{obs} to k_{cap} can be used to obtain the ratio of the two competing unimolecular reactions of the proton-bound dimer, dissociation (k_{diss}) and isomerization (k_{iso}). If the activation energy for the dissociation is known, and appropriate vibrational frequencies are available for the two transition structures, the isomerization activation energy can be adjusted until Eq. 4.1.6 is satisfied.

Ab initio calculations [41] were performed using the Gaussian 98 suite of programs [42]. For each reaction, the proton-bound dimer was optimized at the HF/6-31 G(d) level of theory and vibrational frequencies were calculated and scaled by 0.9135 [43]. The dissociation and isomerization channels were each modelled with the standard RRKM expression:

$$k(E) = \frac{\sigma N^{\neq}(E - E_0)}{h\,\rho(E)} \qquad (4.3.1)$$

where $N^*(E\text{-}E_0)$ and $\rho(E)$ are the sum and density of states of the transition state and reactant ion, respectively. They were calculated employing the direct-count algorithm developed by Beyer and Swinehart as described in [34]. Transition state frequencies were taken to be the same as those of the reactant dimer ion, with one removed to represent the motion over the col. The lowest frequencies were then scaled to yield an entropy of activation, ΔS^* (600 K) of +12 J K^{-1} mol^{-1} for a dissociation reaction and -12 J K^{-1} mol^{-1} for an isomerization reaction (typical values for these processes). The vibrational frequencies are listed in Table 4.3.1.

Table 4.3.1

Vibrational frequencies used in the RRKM modelling of the dissociation and isomerization reactions of the proton-bound dimer ions[a].

System	unique modes	common modes
$(CH_3OH)_2H^+$	42, 71, 96, 113, 151	285, 358, 469, 879, 958, 988, 1044, 1160, 1172, 1199, 1305, 1394, 1461, 1484, 1486, 1492, 1496, 1511, 1682, 2308, 2975, 3005, 3060, 3070, 3114, 3127, 3659, 3728.
TS (diss)	(-311)[b], 26, 44, 60, 70, 94	
TS (iso)	(-1044)[b], 53, 90, 121, 143, 191	
$(CH_3CH_2OH)_2H^+$	24, 44, 65, 83, 115	238, 260, 276, 361, 383, 407, 486, 762, 806, 808, 858, 952, 971, 1017, 1049, 1118, 1146, 1180, 1233, 1296, 1302, 1327, 1400, 1419, 1440, 1461, 1482, 1490, 1499, 1501, 1511, 1529, 1700, 2506, 2933, 2953, 2979, 2988, 3017, 3019, 3026, 3033, 3033, 3094, 3660, 3728.
TS (diss)	(-486)[b], 15, 27, 41, 52, 72	
TS (iso)	(-1017)[b], 30, 55, 82, 104, 144	
$(CH_3OH)(CH_3CH_2OH)H^+$	36, 65, 75, 90, 141	243, 279, 365, 383, 469, 757, 806, 945, 969, 996, 1037, 1144, 1150, 1173, 1243, 1301, 1390, 1402, 1440, 1482, 1489, 1497, 1499, 1510, 1512, 1698, 2573, 2953, 2972, 3019, 3025, 3033, 3054, 3065, 3094, 3657, 3731.
TS (diss)	(-469)[b], 22, 40, 46, 56, 87	
TS (iso)	(-996)[b], 45, 81, 93, 113, 176	

$(CH_3OH)(CH_3CH_2CH_2OH)H^+$	26, 35, 69, 79, 117	140, 202, 253, 325, 353, 448, 489, 728, 804, 855, 893, 960, 1000, 1024, 1049, 1108, 1166, 1175, 1218, 1287, 1304, 1385, 1391, 1424, 1443, 1480, 1488, 1496, 1498, 1503, 1509, 1512, 1687, 2574, 2934, 2942, 2972, 2972, 3004, 3020, 3020, 3054, 3064, 3090, 3657, 3733.
TS (diss)	(-489)[b], 16, 22, 43, 49, 73	
TS (iso)	(-1000)[b], 32, 44, 86, 98, 146	
$(CH_3CH_2OH)(CH_3CH_2CH_2OH)H^+$	18, 36, 56, 92, 105	145, 208, 240, 277, 292, 329, 386, 454, 481, 755, 772, 806, 834, 903, 930, 957, 975, 1044, 1073, 1118, 1146, 1164, 1231, 1274, 1288, 1306, 1350, 1389, 1402, 1437, 1439, 1456, 1482, 1488, 1497, 1499, 1504, 1511, 1524, 1695, 2429, 2930, 2934, 2952, 2967, 2977, 2992, 3009, 3018, 3022, 3026, 3033, 3091, 3657, 3738.
TS (diss)	(-481)[b], 11, 22, 35, 57, 65	
TS (iso)	(-1044)[b], 22, 45, 70, 116, 132	
$(CH_3CH_2CH_2OH)_2H^+$	17, 32, 34, 65, 78	124, 136, 187, 227, 227, 272, 289, 352, 425, 471, 481, 747, 752, 820, 874, 881, 884, 895, 968, 989, 1011, 1024, 1068, 1125, 1145, 1193, 1220, 1256, 1286, 1318, 1322, 1337, 1354, 1390, 1427, 1436, 1438, 1446, 1493, 1494, 1500, 1501, 1507, 1509, 1512, 1520, 1685, 2393, 2926, 2935, 2935, 2941, 2965, 2974, 2985, 2993, 3005, 3013, 3017, 3023, 3027, 3089, 3662, 3723.
TS (diss)	(-480)[b], 11, 20, 21, 40, 49	
TS (iso)	(-989)[b], 22, 40, 43, 81, 98	
$((CH_3)_2CHOH)_2H^+$	12, 27, 37, 76, 97	209, 222, 229, 261, 271,338, 350, 353, 382, 412, 449, 465, 500, 690, 784, 859, 919, 934, 936, 943, 944, 963, 1056, 1113, 1128, 1139, 1172, 1195, 1231, 1302, 1371, 1380, 1386, 1404, 1435, 1441, 1445, 1447, 1478, 1485, 1485, 1492, 1495, 1499, 1503, 1508, 1702, 2545, 2933, 2937, 2941, 2945, 2977, 2993, 3001, 3008, 3009, 3011, 3019, 3021, 3032, 3058, 3658, 3730.
TS (diss)	(-500)[b], 8, 17, 23, 47, 60	
TS (iso)	(-963)[b], 16, 34, 46, 95, 122	

[a] Common modes are used for the reactant ion and both transition states.
[b] Common mode removed to represent the motion over the col.

4.3.1 $CH_3OH + CH_3OH_2^+$

Since the proton-bound dimer ion was not observed in any of the mass spectra obtained for this reaction, we can use a simplified version of Eq. 4.1.6:

$$\frac{k_{iso}}{k_{iso} + k_{diss}} = \frac{k_{obs}}{\rho_{cap} k_{cap}} \tag{4.3.2}$$

The activation energy for the dissociation reaction of $(CH_3OH)_2H^+$ was taken from an equilibrium high-pressure mass spectrometry study conducted by Larson and McMahon, 131 ± 8 kJ mol^{-1} [44]. While their values are quoted at 298 K, the thermal correction for the reactants and dimer essentially cancel out. Thus, their 298 K values are used throughout this work. If CH_3OH and $CH_3OH_2^+$ in the ion trap are initially at 298K, then we need to extract from the RRKM modelling the k_{diss} and k_{iso} corresponding to an internal energy of the proton-bound dimer of 153 kJ mol^{-1} (131 kJ mol^{-1} plus the average thermal internal energy of the two reactants). Then by fixing $\Delta S^{\ddagger}$ (600 K) for the two unimolecular channels (-12 J K^{-1} mol^{-1} and + 12 J K^{-1} mol^{-1} for the isomerization and dissociation processes, respectively), the only adjustable parameter becomes the activation energy for the isomerization channel. This value can be adjusted so that Eq. 4.3.2 is satisfied. With this procedure, the E_o for the isomerization process was determined to be 132 ± 2 kJ mol^{-1} (Table 4.3.2). It should be noted that the quoted precision of this value was determined primarily by the precision in E_{diss} quoted by Larson and McMahon [44], and as such, should be considered a minimum value for the uncertainty.

This result compares reasonably well with the theoretical value of 125 kJ mol^{-1} calculated by Bouchoux and Choret [16] using the MP2/6-31G* level of theory. Alternatively, the theoretical value of 125 kJ mol^{-1} can be used to derive k_{iso} and therefore k_{obs}. A value of 5.5 x 10^{-10} cm^3 $molecule^{-1}$ s^{-1} was obtained for k_{obs}, which is five times greater than that measured with the ion trap. Agreement can be forced by altering the effective temperature of the system, but this results in a value of 147 K for the reactant ion and neutral.

4.3.2 Other systems

The mass spectra of all the other reaction systems studied contained the intact proton-bound dimer and so Eq.4.1.6 must be used. The rate constant for collisional stabilization of the initially formed excited complex, k_s [M] was calculated to be 1.75 x 10^4 cm^3 $molecule^{-1}$ s^{-1} based upon the polarizability of the helium atom (0.20 x 10^{-24} cm^3) [39] and a helium pressure of 1 mTorr. The extraction of E_{iso} for the initially formed proton-bound dimer was done in a manner similar to that described above for the $CH_3OH_2^+ + CH_3OH$ reaction. The vibrational frequencies employed in the RRKM analysis are listed in Table 4.3.1. The values for E_{diss} were all either experimentally measured by Larson and McMahon [44], or derived using the empirical formula developed by them for asymmetric proton-bound dimers. All values can be found in Table 4.3.2.

An S_N2-type mechanism has been established in the literature for the dehydration of these proton-bound alcohol dimers. It has been confirmed for the methanol dimer by experiments [28] and theory [16-18] and experiments also suggest this type of mechanism for the propanol dimers

[23]. The present results also support this general mechanism. In these proton-bound alcohol dimers, there exists a small barrier to the classical S_N2 transition state $(RO(H)\bullet\bullet\bullet R'\bullet\bullet\bullet OH_2^+)^{\ddagger}$, which subsequently collapses to the intermediate $RO(H)\text{-}R'\bullet\bullet\bullet OH_2^+$. This intermediate, consisting of a protonated ether solvated with water, has excess energy and thus, decomposes by elimination of water.

The value of E_{iso} decreases as the size of the alkyl groups in the reacting system increases. This is most evident in the series of reactions involving protonated n-propanol and the homologous series of alcohols: methanol, ethanol and n-propanol. The value of E_{iso} drops by 14 kJ mol^{-1} across the series, which is consistent with greater charge stabilization in the intermediate $[RO(H)\bullet\bullet\bullet R'OH_2]^+$ and $[RO(H)\text{-}R'\bullet\bullet\bullet OH_2]^+$ complexes. The trend is also consistent with a weaker $R'\text{-}OH_2$ bond strength as the size of R' increases, which is expected if the water loss occurs from the methanol, ethanol and n-propanol moieties. This would need to be confirmed with isotopic labelling experiments.

Table 4.3.2

Isomerization barriers extracted for the systems in this study.

Proton-bound dimer	E_{diss} [a,b]	E_{iso} [a,c]
$(CH_3OH)(CH_3OH)H^+$	131	132 (125)[d]
$(CH_3CH_2OH)(CH_3OH)H^+$	122	128
$(CH_3CH_2OH)(CH_3CH_2OH)H^+$	131	126
$(CH_3CH_2CH_2OH)(CH_3OH)H^+$	123	123
$(CH_3CH_2CH_2OH)(CH_3CH_2OH)H^+$	126	118
$(CH_3CH_2CH_2OH)(CH_3CH_2CH_2OH)H^+$	131	109
$((CH_3)_2CHOH)((CH_3)_2CHOH)H^+$	131	107

[a] Values in kJ mol^{-1}.

[b] Reference [44] quoted uncertainty ± 8 kJ mol^{-1}.

[c] Minimum uncertainty ± 2 kJ mol^{-1} (see text).

[d] Reference [16].

4.4 Conclusion

A Finnigan GCQ ion trap mass spectrometer was used to measure the rate constants for the ion/molecule reactions involving protonated and neutral alcohols. RRKM modelling of the unimolecular reactions of the initially formed excited proton-bound dimer allowed the activation energy for the isomerization of the proton-bound dimers to be determined. These values decrease with increasing size of the dimer, which is consistent with the previously proposed S_N2-type mechanism for the reaction, which ultimately leads to the loss of a molecule of water. The ion trap can therefore be used to quickly and reliably determine the energetics of processes on a complex potential energy surface.

References

[1] P. Kebarle, in Techniques for the Study of Ion/molecule Reactions, J.M. Farrar and W.H.Saunders (Ed), Wiley-Interscience, New York, 1988.

[2] M. Meot-Ner, J. Am. Chem. Soc. 106 (1984) 1265-1272.

[3] K. Hiraoka, H. Takimoto and S. Yamabe, J. Phys. Chem. 90 (1986) 5910-5914.

[4] A. W. Castleman and S. Wei, Annu. Rev. Phys. Chem. 45 (1994) 685-719.

[5] A. W. Castleman and K. H. Bowen, J. Phys. Chem. 100 (1996) 12911-12944.

[6] E. E. Ferguson, F. C. Fehsenfeld and D. L. Albritton, in Gas Phase Ion Chemistry, M.T. Bowers (Ed), Academic Press, New York,1979.

[7] S. Hammerum, NATO ASI Ser., Ser. C, 347 (1991) 379-90.

[8] D. Harnish and J. L. Holmes, J. Am. Chem. Soc. 113 (1991) 9729-9734.

[9] T. H. Morton, Org. Mass Spectrom. 26 (1991) 18-23.

[10] N. Heinrich and H. Schwarz, in Ion and Cluster Ion Spectroscopy, Elsevier, Amsterdam,1989.

[11] G. Schaftenaar, R. Postma, P. J. A. Ruttink, P. C. Burgers, G. A. McGibbon and J. K. Terlouw, Int. J. Mass Spectrom. Ion Proc. 100 (1990) 521.

[12] J. L. Holmes, C. E. C. A. Hop and J. K. Terlouw, Org. Mass Spectrom. 21 (1986) 776.

[13] J. A. Booze and T. Baer, J. Phys. Chem. 96 (1992) 5715-5719.

[14] P. M. Mayer and T. Baer, J. Phys. Chem. 36 (1996) 14949-14957.

[15] O. A. Mazyar, P. M. Mayer and T. Baer, Int. J. Mass Spectrom. Ion Proc. 167/168 (1997) 389-402.

[16] G. Bouchoux and N. Choret, Rapid. Commun. Mass Spectrom. (1997) 1799-1807.

[17] K. Raghavachari, J. Chandrasekhar and R. C. Burnier, J. Am. Chem. Soc. 106 (1984) 3124-3128.

[18] J. C. Sheldon, G. J. Currie and J. H. Bowie, J. Chem. Soc. Perkin Trans. II (1986) 941-944.

[19] Z. Karpas and M. Meot-Ner, J. Phys. Chem. 93 (1989) 1859-1863.

[20] S. Morgan, R. G. Keesee and J. A. E. Castleman, J. Am. Soc. Chem. 111 (1989) 3841-3845.

[21] F. Mafune, J. Kohno and T. Kondow, J. Phys. Chem. 100 (1996) 10041-10045.

[22] S. T. Graul and R. R. Squires, Int. J. Mass Spectrom. 81 (1987) 183-202.

[23] H. E. Audier, C. Monteiro, P. Mourgues and D. Robin, Rapid Commun. Mass Spectrom. 3 (1989) 84-86.

[24] L. M. Bass, R. D. Cates, M. F. Jarrold, N. J. Kirchner and M. T. Bowers, J. Am. Soc. Chem. 105 (1983) 7024-7033.

[25] J. C. Kleingeld and N. M. M. Nibbering, Org. Mass Spectrom. 17 (1982) 136-138.

[26] T. T. Dang and V. M. Bierbaum, Int. J. Mass Spectrom. 117 (1992) 65-82.

[27] J. M. Tedder and G. S. Walker, J. Chem. Soc. Perkin Trans. 2 (1991) 317-320.

[28] R. A. Morris, A. A. Viggiano, J. F. Paulson and M. J. Henchman, J. Am. Soc. Chem. 113 (1991) 5932-5936.

[29] T. B. McMahon and J. L. Beauchamp, J. Phys. Chem. 81 (1977) 593-598.

[30] M. Meot-Ner, in Gas-Phase Ion Chemistry, M. T. Bowers (Ed), Academic Press, New York, 1979.

[31] M. Meot-Ner and F. H. Field, J. Am. Chem. Soc. 97 (1975) 5339-5344.

[32] T. Su and W. J. Chesnavich, J. Chem. Phys. 76 (1982) 5183-5185.

[33] T. Su and M. T. Bowers, J. Chem. Phys. 58 (1973) 3027-3037.

[34] T. Baer and W. L. Hase, Unimolecular Reaction Dynamics, Theory and Experiments, Oxford University Press, New York, 1996.

[35] R. Grover, M. Decouzon, P.-C. Maria and J.-F. Gal, Eur. Mass Spectrom. 2 (1996) 213-223.

[36] R. Carpignano, L. Operti, R. Rabezzana and G. A. Vagglio, J. Am. Soc. Mass Spectrom. (1998) 938-944.

[37] J. E. Bartmess and R. M. Georgiadis, Vacuum 33 (1983) 149-153.

[38] F. Mafune, J. Kohno and T. Kondow, J. Phys. Chem. 100 (1996) 10041-10045.

[39] T. M. Miller, in CRC Handbook of Chemistry and Physics, R.C. Weast (Ed), CRC Press, Florida,1987.

[40] J. R. D. Nelson, J. D. R. Lide and A. A. Maryott, in CRC Handbook of Chemistry and Physics R.C. Weast (Ed), CRC Press, Florida,1987.

[41] W. J. Hehre, L. Radom, P. v. R. Schleyer and J. A. Pople, Ab Initio Molecular Orbital Theory, Wiley, New York, 1986.

[42] M. J. Frisch, G. W. Trucks, H. B. Schlegel, G. E. Scuseria, M. A. Robb, J. R. Cheeseman, V. G. Zakrzewski, J. A. Montgomery, R. E. Stratmann, J. C. Burant, S. Dapprich, J. M. Millam, A. D. Daniels, K. N. Kudin, M. C. Strain, O. Farkas, J. Tomasi, V. Barone, M. Cossi, R. Cammi, B. Mennucci, C. Pomelli, C. Adamo, S. Clifford, J. Ochterski, G. A. Petersson, P. Y. Ayala, Q. Cui, K. Morokuma, D. K. Malick, A. D. Rabuck, K.

Raghavachari, J. B. Foresman, J. Cioslowski, J. V. Ortiz, B. B. Stefanov, G. Liu, A. Liashenko, P. Piskorz, I. Komaromi, R. Gomperts, R. L. Martin, D. J. Fox, T. Keith, M. A. Al-Laham, C. Y. Peng, A. Nanayakkara, C. Gonzalez, M. Challacombe, P. M. W. Gill, B. Johnson, W. Chen, M. W. Wong, J. L. Andres, C. Gonzalez, M. Head-Gordon, E. S. Replogle and J. A. Pople *GAUSSIAN 98 Rev. A.7*; Gaussian Inc.: Pittsburgh PA, 1998.

[43] A. P. Scott and L. Radom, J. Phys. Chem. 100 (1996) 16502-16513.

[44] J. W. Larson and T. B. McMahon, J. Am. Chem. Soc. 104 (1982) 6255-6261.

Chapter 5

The Energetics of the Dehydration of Nitrile-Alcohol Proton-Bound Dimers

5.1 Introduction

The family of proton-bound mixed dimers consisting of nitriles and alcohols all have at least one common feature, they exhibit in their unimolecular chemistry the competition between simple-bond dissociations and dehydration reactions [1]. The dehydration of these simple clusters necessarily involves the isomerization of the proton-bound entity, as shown below in Fig. 5.1.1 for the proton-bound dimer of acetonitrile and methanol.

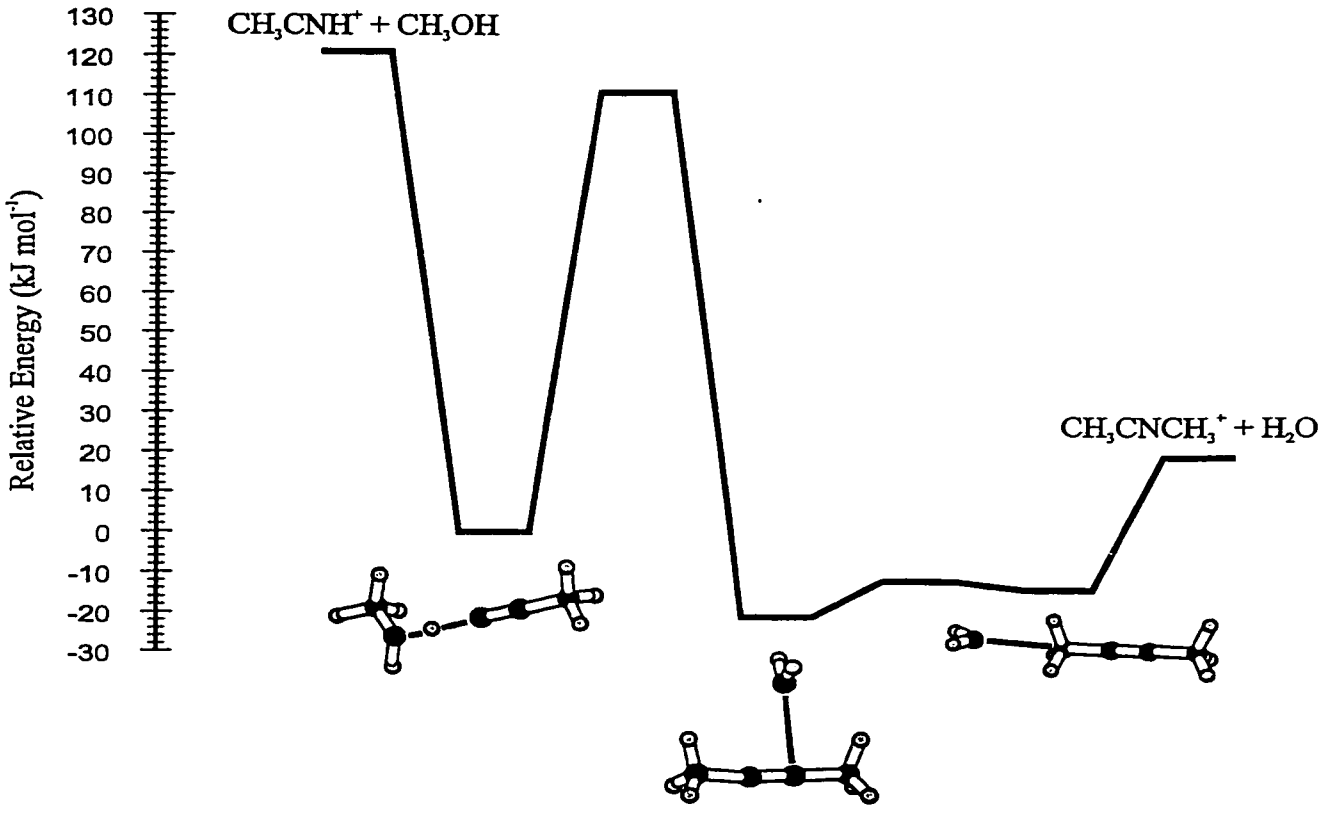

Fig 5.1.1 Potential Energy Surface of the Methanol-Acetonitrile Proton Bound Dimer

The isomerization of these clusters will also have an impact on the kinetics of the reactions between ions and molecules in the gas phase. Even though there is no activation barrier to an ion/molecule reaction, the presence of the isomerization barrier on the reaction surface can make the reaction less efficient. The cluster surface in Fig. 5.1.1 can also be viewed from the point of view of an ion/molecule reaction.

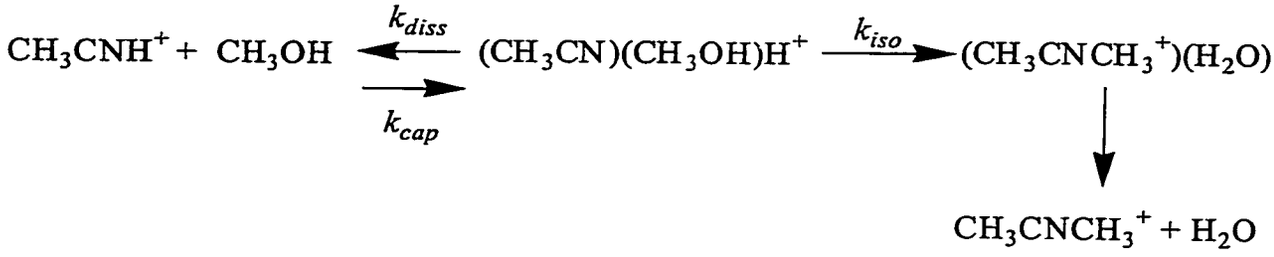

As seen in the previous chapter, the observed forward rate constant, k_{obs}, for the reactions studied (leading to the dehydration products) can be written as [2]:

$$k_{obs} = \rho_{cap} k_{cap} \left(\frac{k_{iso}}{k_{iso} + k_{diss} + k_s[M]} \right) \qquad (5.1.1)$$

where k_{iso} is the rate constant for the isomerization of the dimer ions (which eventually leads to the loss of water) and k_{diss} is the rate constant for the dissociation reaction of the dimer (both of which can be calculated using RRKM theory [3]). The probability that a collision will lead to a long-lived excited intermediate complex is referred to as ρ_{cap} (the association reaction can normally be assumed to occur on every collision and ρ_{cap} is then assumed to be unity), while k_{cap} is the rate constant for capture collisions occurring between the reactant ion and neutral

(calculated using the ion-dipole theory of Su and Chesnavich) [4] and k_s[M] is the rate constant for collisional stabilization of the initially formed excited complex calculated employing the ion-induced dipole theory developed by Langevin [5]. k_s[M] will depend on the pressure in the reaction chamber.

In the present study an ion trap mass spectrometer is used to measure the bimolecular rate constants for reactions between protonated acetonitrile and methanol and ethanol, and for the reaction between protonated n-propanol and acetonitrile. The goal is to compare the experimentally determined values with those obtained from theory, and to extract information about the cluster ion isomerization barrier.

5.2 Computational Methods

Ab initio calculations [6] were performed using the Gaussian 98 suite of programs [7]. For the two reactions involving protonated acetonitrile, the corresponding dimer ions $(CH_3CN)(CH_3OH)H^+$ and $(CH_3CN)(CH_3CH_2OH)H^+$, have been modelled previously in our group at the MP2/6-31+G(d) level of theory [1,8]. Vibrational frequencies for these dimers were taken from those studies. The dimer $(CH_3CN)(CH_3CH_2CH_2OH)H^+$, was optimized in the present study at the HF/6-31G(d) level of theory and vibrational frequencies (scaled by 0.9135) calculated at this level were used in the RRKM modelling for this system. The dissociation energy for this dimer was estimated at the MP2/6-31 +G(d) level of theory.

The dissociation and isomerization channels for each dimer ion were modelled with the standard RRKM expression:

$$k(E) = \frac{\sigma N^{*}(E - E_0)}{h\,\rho(E)} \qquad (5.2.1)$$

where $N^{*}(E-E_0)$ and $\rho(E)$ are the sum and density of states of the transition state and reactant ion, respectively. They were calculated employing the direct-count algorithm developed by Beyer and Swinehart [3]. Transition state frequencies were taken to be the same as those of the reactant dimer ion, with one removed to represent the motion over the col. The lowest frequencies were then scaled to yield an entropy of activation, $\Delta S^{*}(600\ K)$ of $+12\ J\ K^{-1}\ mol^{-1}$ for a dissociation reaction and $-12\ J\ K^{-1}\ mol^{-1}$ for an isomerization reaction. The vibrational frequencies are listed in Table 5.3.2.

5.3 Results and Discussion

5.3.1 Determining k_{obs}

The procedure for determining the bimolecular rate constants, k_{obs}, for the three ion/molecule reactions discussed in this study is outlined below. The results are summarized in Table 5.3.1, which includes the theoretical collision capture rate constants, k_{cap}, for comparison.

5.3.1.1 $CH_3CNH^+ + CH_3OH$

The reaction between protonated acetonitrile and neutral methanol

$$\underset{\text{m/z 42}}{CH_3CNH^+} + CH_3OH \rightarrow \underset{\text{m/z 56}}{CH_3CNCH_3^+} + H_2O$$

occurs on the potential energy surface presented in Fig. 5.1.1. The peak heights of the m/z 42 and m/z 56 ions (Fig. 5.3.1) were measured and a plot of ln $[H_{42} / (H_{42} + H_{56})]$ vs. reaction time was made for each different methanol pressure studied (1.4×10^{-6} Torr, 2.9×10^{-6} Torr, 4.9×10^{-6} Torr, 8.6×10^{-6} Torr and 1.2×10^{-5} Torr). The slope from each plot yielded pseudo-first order rate constants (Fig. 5.3.2(a)). These rate constants were then plotted against their respective methanol pressures to yield the bimolecular rate constant of $(4.6 \pm 0.2) \times 10^{-11}$ $cm^3 molecule^{-1} s^{-1}$ (Fig. 5.3.2(b)). The error is based upon five different experiments, but does not include errors due to assumptions made in the kinetic treatment such as a unity value for ρ_{cap}, and thus should be taken as a minimum error. This value is two orders of magnitude lower than k_{cap}, 2.3×10^{-9} cm^3 $molecule^{-1}$ s^{-1} (obtained using the ion-dipole theory of Su and Chesnavich [4]). The polarizability and the dipole moment of methanol were obtained from the literature [9,10]. This indicates that the presence of the isomerization barrier for the $(CH_3CN)(CH_3OH)H^+$ dimer ion hinders the ion/molecule reaction by creating a bottle-neck in the overall availability of states for the reaction as it progresses from reactants to products.

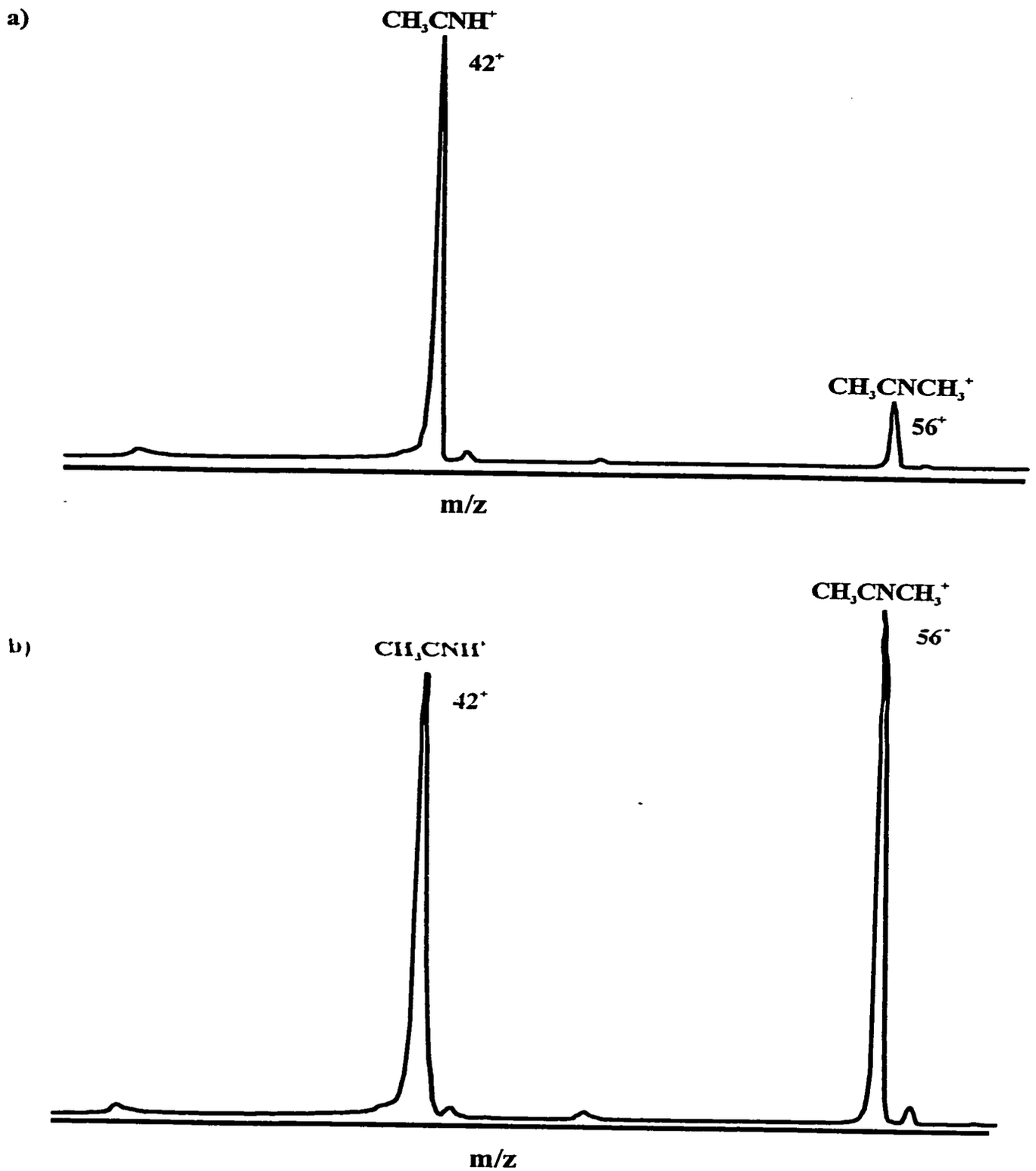

Fig. 5.3.1. Mass spectra corresponding to reaction times a) 1 ms and b) 30 ms for the ion/molecule reaction between CH_3CNH^+ and CH_3OH.

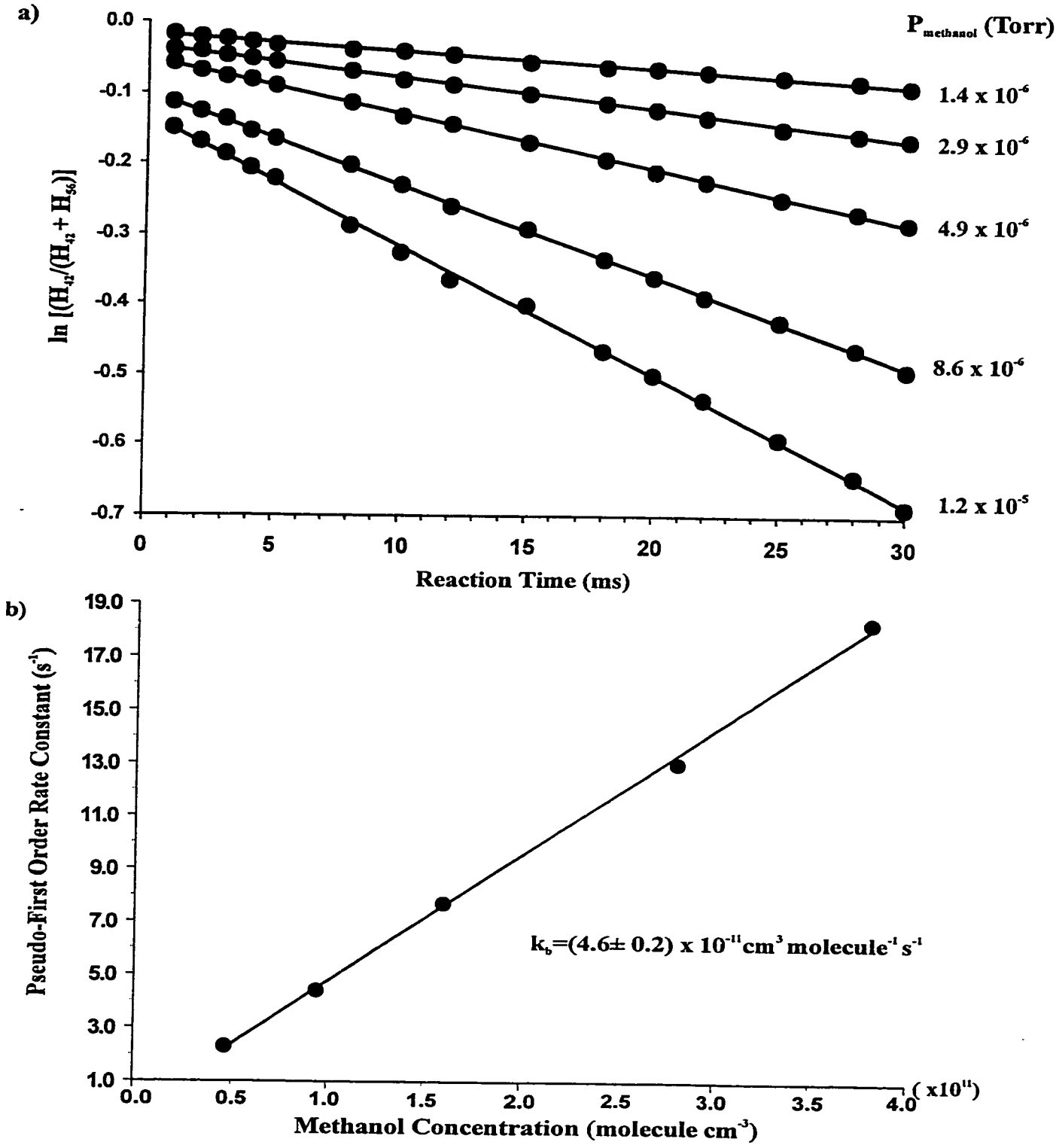

Fig 5.3.2 a) Pseudo-first order plots for the reaction $CH_3CNH^+ + CH_3OH \rightarrow CH_3CNCH_3^+ + H_2O$ at five neutral methanol pressures, b) Plot of the pseudo-first order rate constant as a function of methanol pressure. No error bars were placed on the graph as the experimental uncertainty of the data points was smaller than the points themselves.

5.3.1.2 $CH_3CNH^+ + CH_3CH_2OH$

The mass spectrum resulting from the ion/molecule reaction between CH_3CNH^+ and CH_3CH_2OH in the ion trap exhibits two peaks, m/z 42 (CH_3CNH^+) and m/z 70 ($CH_3CNCH_2CH_3^+$). A small peak at m/z 47 ($CH_3CH_2OH_2^+$) was minimized by increasing the pressure of CH_3CN. In the ensuing kinetic treatment, the original concentration of CH_3CNH^+ was approximated by the sum of the two peaks with m/z 42 and m/z 70 in the mass spectrum. The peak heights of m/z 42 and m/z 70 ions were measured and a plot of $\ln[H_{42}/(H_{42}+H_{70})]$ vs. reaction time was made for each different ethanol pressure (Fig. 5.3.3(a)). A corrected experimental bimolecular rate constant value of $(3.9 \pm 0.4) \times 10^{-10}$ cm^3 molecule^{-1} s^{-1} was obtained (Fig. 5.3.3(b)), which is an order of magnitude smaller than k_{cap} (2.2×10^{-9} cm^3 molecule^{-1} s^{-1}) [4].

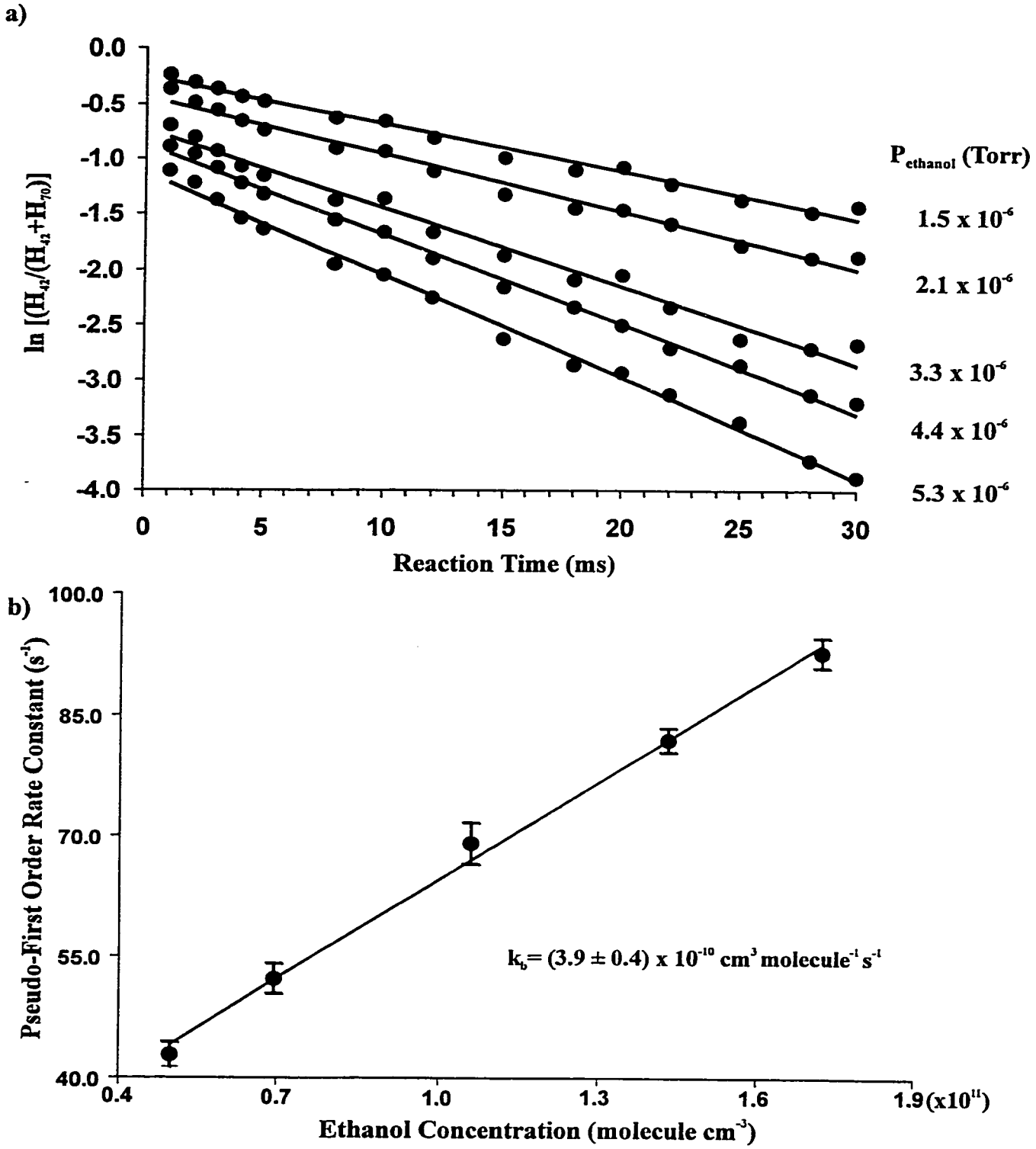

Fig 5.3.3 a) Pseudo-first order plots for the reaction $CH_3CNH^+ + CH_3CH_2OH \rightarrow CH_3CNCH_2CH_3^+ + H_2O$ at five different ethanol pressures, b) Plot of pseudo-first order rate constant as a function of ethanol pressure.

5.3.1.3 $CH_3CH_2CH_2OH_2^+ + CH_3CN$

The reaction between protonated n-propanol and neutral acetonitrile

$$\underset{\text{m/z 61}}{CH_3CH_2CH_2OH_2^+} + CH_3CN \rightarrow \underset{\text{m/z 84}}{CH_3CH_2CH_2CNCH_3^+} + H_2O$$

results in three peaks in the mass spectrum, m/z 61 ($CH_3CH_2CH_2OH_2^+$), m/z 84 ($CH_3CH_2CH_2CNCH_3^+$) and the proton-bound dimer, m/z 102 $(CH_3CN)(CH_3CH_2CH_2OH)H^+$. The original concentration of $CH_3CH_2CH_2OH_2^+$ was approximated from the sum of all three peaks in the mass spectrum. The peak heights of m/z 61, m/z 84 and m/z 102 ions were measured and a plot of $\ln [(H_{61})/(H_{61}+H_{84}+H_{102})]$ vs. reaction time was made for each acetonitrile pressure (Fig. 5.3.4(a)). A bimolecular rate constant of $(2.1 \pm 0.4) \times 10^{-10}$ cm^3 molecule^{-1} s^{-1} was obtained (Fig. 5.3.4(b)), which is also approximately an order of magnitude lower than k_{cap} (3.7×10^{-9} cm^{3}molecule^{-1}s^{-1}) [4]. Note the change in k_{cap} when acetonitrile is the neutral reagent (due to its greater dipole moment and polarizability).

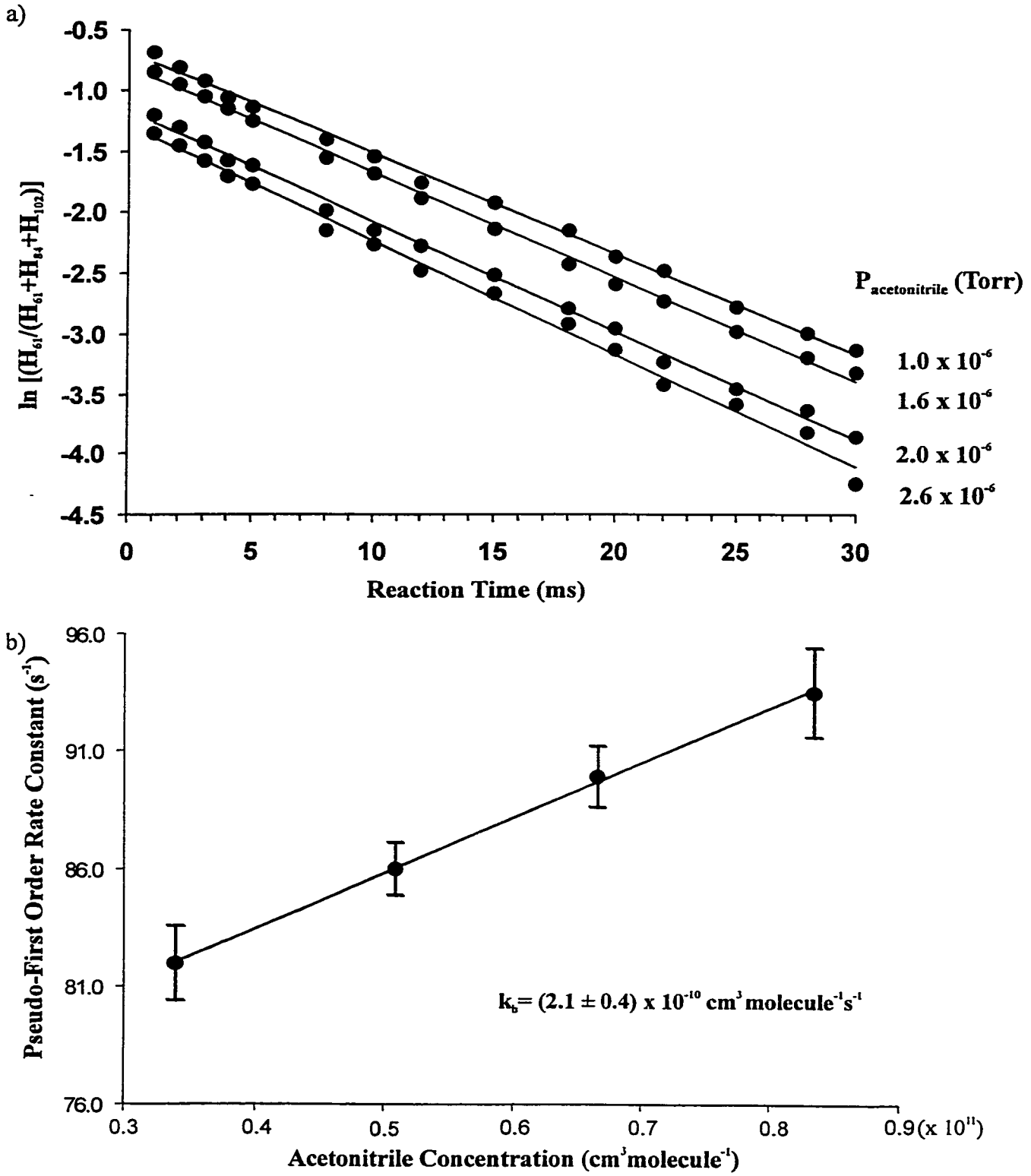

Fig 5.3.4 a) Pseudo-first order plots for the reaction $CH_3CH_2CH_2OH_2^+ + CH_3CN \rightarrow$ m/z 102 + H_2O for four different CH_3CN pressures, b) Plot of the pseudo-first order rate constant as a function of acetonitrile pressure.

Table 5.3.1

Comparison of the measured ion/molecule reaction rate constant, k_{obs}, with that predicted by collision theory, k_{cap}, for reactions leading to formation of neutral water [a].

Reaction	k_{obs}	k_{cap} [b]
$CH_3CNH^+ + CH_3OH$	0.046 ± 0.002	2.3
$CH_3CNH^+ + CH_3CH_2OH$	0.39 ± 0.04	2.2
$CH_3CH_2CH_2OH_2^+ + CH_3CN$	0.21 ± 0.04	3.7

[a] Rate constants are in units of 10^{-9} cm^3 $molecule^{-1}$ s^{-1}.

[b] Using the theory described by Su and Chesnavich [4].

5.3.2 The isomerization barrier energy

The rate constants derived above can be used to extract information about the reaction surface. Referring to Eq. 5.1.1, the ratio of k_{obs} to k_{cap} can be used to obtain the ratio of the two competing unimolecular reactions of the proton-bound dimer, dissociation (k_{diss}) and isomerization (k_{iso}). If the activation energy of the dissociation is known, and appropriate vibrational frequencies are available for the two transition structures, the isomerization activation energy can be adjusted until Eq.5.2.1 is satisfied. In previous work from this laboratory, the unimolecular reactions of the proton-bound dimers, $(CH_3CN)(CH_3OH)H^+$ and $(CH_3CN)(CH_3CH_2OH)H^+$, encountered in the present study were investigated [1,8]. High level ab initio calculations were used to model the unimolecular reaction surfaces and estimate their respective dissociation energies. Calculated vibrational frequencies were used to model the isomerization channel with RRKM theory [3], and to extract isomerization barrier energies. To

do this, the log$k(E)$ vs E curves for dissociation and isomerization were adjusted to achieve an overlap that appeared reasonable based on the mass spectrum of metastable (low internal energy) dimer ions. The values that were obtained in this manner are summarized in Table 5.3.3. The vibrational frequencies quoted in those works [1,8] were used in the present study in the modelling of k_{obs} for these two dimer ions.

Table 5.3.2

Vibrational frequencies used in the RRKM modelling of the dissociation and isomerization reaction of the $(CH_3CN)(CH_3CH_2CH_2OH)H^+$ proton-bound dimer. [a]

System	Harmonic Vibrational Frequencies (cm^{-1})
$(CH_3CN)(CH_3CH_2CH_2OH)H^+$	3 ,34 ,39, 87, 108, 122, 171, 227, 282, 404, 413, 432, 460, 753, 807, 869, 878, 893, 940, 1008, 1067, 1071, 1072, 1159, 1214, 1283, 1321, 1355, 1423, 1427, 1438, 1462, 1462, 1494, 1500, 1507, 1512, 1716, 2401, 2791, 2936, 2942, 2960, 2986, 3006, 3020, 3024, 3044, 3044, 3093, 3650
TS (diss)	(-460)[b], 2, 21, 24, 54, 67, 122, 171, 227, 282, 404, 413, 432, 753, 807, 869, 878, 893, 940, 1008, 1067, 1071, 1072, 1159, 1214, 1283, 1321, 1355, 1423, 1427, 1438, 1462, 1462, 1494, 1500, 1507, 1512, 1716, 2401, 2791, 2936, 2942, 2960, 2986, 3006, 3020, 3024, 3044, 3044, 3093, 3650
TS (iso)	(-1008)[b], 4, 43, 48, 108, 135, 122, 171, 227, 282, 404, 413, 432, 460, 753, 807, 869, 878, 893, 940, 1067, 1071, 1072, 1159, 1214, 1283, 1321, 1355, 1423, 1427, 1438, 1462, 1462, 1494, 1500, 1507, 1512, 1716, 2401, 2791, 2936, 2942, 2960, 2986, 3006, 3020, 3024, 3044, 3044, 3093, 3650.

[a] HF/6-31 G(d) values scaled by 0.9135.

[b] Mode removed to represent the motion over the col.

5.3.2.1 $CH_3CNH^+ + CH_3OH$

Since the intact proton-bound dimer ion was not observed in any of the mass spectra obtained for this reaction, we can use a simplified version of Eq. 5.2.1:

$$\frac{k_{iso}}{k_{iso} + k_{diss}} = \frac{k_{obs}}{\rho_{cap} k_{cap}} \tag{5.3.1}$$

where k_{iso} is the rate of isomerization from $(CH_3CN)(CH_3OH)H^+$ to $(CH_3CNCH_3)(H_2O)^+$ in Fig. 5.1.1.

The 0 K binding energy of the $(CH_3CN)(CH_3OH)H^+$ complex was previously calculated to be 121 kJ mol^{-1} [1] at the G2 [11] level of theory. If CH_3CNH^+ and CH_3OH are assumed to be at 298 K, then we need to extract from the RRKM modelling the k_{diss} and k_{iso} corresponding to an internal energy of the proton-bound dimer of 145 kJ mol^{-1} (121 kJ mol^{-1} plus the average thermal internal energy of the two reactants). Then by fixing the $\Delta S^{\ddagger}$ for the two unimolecular channels [1], the only adjustable parameter becomes the activation energy for the isomerization channel. With this procedure, the E_0 value for the isomerization process was determined to be 125 ± 2 kJ mol^{-1}. This is slightly larger than the value of 115 ± 10 kJ mol^{-1} that was estimated from the mass spectrum of metastable proton-bound dimers [1]. The precision of the present value is determined primarily by an estimated precision in E_{diss} of ± 8 kJ mol^{-1} that is typical of G2 theory [11], and as such, should be considered a minimum value for the uncertainty.

5.3.2.2 $CH_3CNH^+ + CH_3CH_2OH$

The unimolecular chemistry of the acetonitrile-ethanol proton-bound dimer has been studied in our laboratory [8] and found to be similar to that of $(CH_3CN)(CH_3OH)H^+$. The dimer exhibits three dissociation channels on the microsecond timescale, cleavage of the two hydrogen bonds to form CH_3CNH^+ and $CH_3CH_2OH_2^+$, and dehydration to form $CH_3CNCH_2CH_3^+$. The two simple dissociation reactions compete because the proton affinity (PA) values of acetonitrile and ethanol are similar (779.2 kJ mol^{-1} and 776.4 kJ mol^{-1}, respectively [12]). The formation of $CH_3CNCH_2CH_3^+$ involves the isomerization of the proton-bound dimer prior to water loss. From an analysis of the relative intensities of the peaks in the mass spectrum of metastable $(CH_3CN)(CH_3CH_2OH)H^+$ ions using RRKM theory, it was evident that the barrier to isomerization for this system was lower (relative to the reactants $CH_3CNH^+ + CH_3CH_2OH$) than was observed for the reaction involving methanol. An estimated value of E_{iso} of 130 ± 10 kJ mol^{-1} was obtained [8].

In the present study, a small peak is observed in the mass spectrum due to the proton-bound dimer, $(CH_3CN)(CH_3CH_2OH)H^+$, m/z 88. However, the bimolecular rate constant was found to be independent of its inclusion in the kinetic treatment, and so Eq. 5.3.1 was again used for determining the isomerization barrier energy.

The 0 K binding energy of the $(CH_3CN)(CH_3CH_2OH)H^+$ complex was previously calculated to be 152 kJ mol^{-1} [8] at the G2(MP2,SVP) level of theory. If CH_3CNH^+ and

CH_3CH_2OH are assumed to be at 298 K, then we need to extract from the RRKM modelling the k_{diss} and k_{iso} corresponding to an internal energy of the proton-bound dimer of 182 kJ mol^{-1} (152 kJ mol^{-1} plus the average thermal internal energy of the two reactants). Employing the vibrational frequencies for the dissociation and isomerization states quoted in Ref. 4, the value of E_{iso} can be adjusted so that Eq. 5.3.1 is satisfied. The E_0 value for the isomerization process was determined to be 142 ± 2 kJ mol^{-1}. This is again slightly larger than the value of 130 ± 10 kJ mol^{-1} that was estimated from the mass spectrum of metastable proton-bound dimers [8].

5.3.2.3 $CH_3CH_2CH_2OH_2^+ + CH_3CN$

The mass spectra of the reaction between protonated n-propanol and neutral acetonitrile contained three peaks, m/z 61 ($CH_3CH_2CH_2OH_2^+$), m/z 84 (due to water loss from the proton-bound dimer) and a significant peak due to the intact proton-bound dimer $(CH_3CN)(CH_3CH_2CH_2OH)H^+$, m/z 102 and thus, Eq. 5.3.1 must be used. The stabilization rate constant, k_s[He], was calculated to be 1.75 x 10^4 cm^{3}molecule^{-1}s^{-1}, based upon the polarizability of the helium atom (0.20 x 10^{-24} cm^3) [9] and a helium pressure of 1 mTorr.

The 0 K binding energy of the $(CH_3CN)(CH_3CH_2CH_2OH)H^+$ complex (relative to $CH_3CH_2CH_2OH_2^+ + CH_3CN$) was calculated in the present study to be 131 kJ mol^{-1} at the MP2/6-31+G(d) level of theory. If CH_3CN and $CH_3CH_2CH_2OH_2^+$ are assumed to be at 298K, then to satisfy Eq. 5.1.1, we need to extract from the RRKM modelling the k_{diss} and k_{iso} corresponding to an internal energy of the proton-bound dimer of 162 kJ mol^{-1} (131 kJ mol^{-1} plus

the average thermal internal energy of the two reactants). The E_0 value for the isomerization process that ultimately satisfies Eq. 5.1.1 was found to be 125 ± 2 kJ mol^{-1}. This value can be compared with an estimate based on the MI mass spectrum of metastable $(CH_3CN)(CH_3CH_2CH_2OH)H^+$ ions (Fig.5.3.5). The MI mass spectrum exhibits two major peaks, m/z 61 and m/z 84 in nearly a 1:1 ratio. Two minor peaks are present at m/z 42 (CH_3CNH^+) and m/z 60 (propene loss). The log k(E) vs. E curves for the dissociation and isomerization reactions of the proton-bound dimer can be adjusted so that they cross in the internal energy range of the dimer appropriate for observations in the second field-free region of the ZAB mass spectrometer. The estimated value of E_{iso} that results is 114 ± 10 kJ mol^{-1}, which is 11 kJ mol^{-1} lower than that predicted from the ion/molecule reaction modelling.

Table 5.3.3

Comparison of the 0 K isomerization activation energy (E_{iso}) obtained from RRKM modelling of metastable ion (MI) mass spectra of proton-bound dimers with those obtained from the present study.

Proton-bound dimer	E_{diss} [a,b]	E_{iso} [a]	
		MI[c]	Present Work
$(CH_3CN)(CH_3OH)H^+$	121 [1]	115 ± 10 [1]	125 ± 2
$(CH_3CN)(CH_3CH_2OH)\ H^+$	152 [8]	130 ± 10 [8]	142 ± 2
$(CH_3CN)(CH_3CH_2CH_2OH)H^+$	131	114 ± 10	125 ± 2

[a] Values in kJ mol^{-1}.

[b] See text.

[c] Estimated based upon relative peak heights in MI mass spectra of proton-bound dimers.

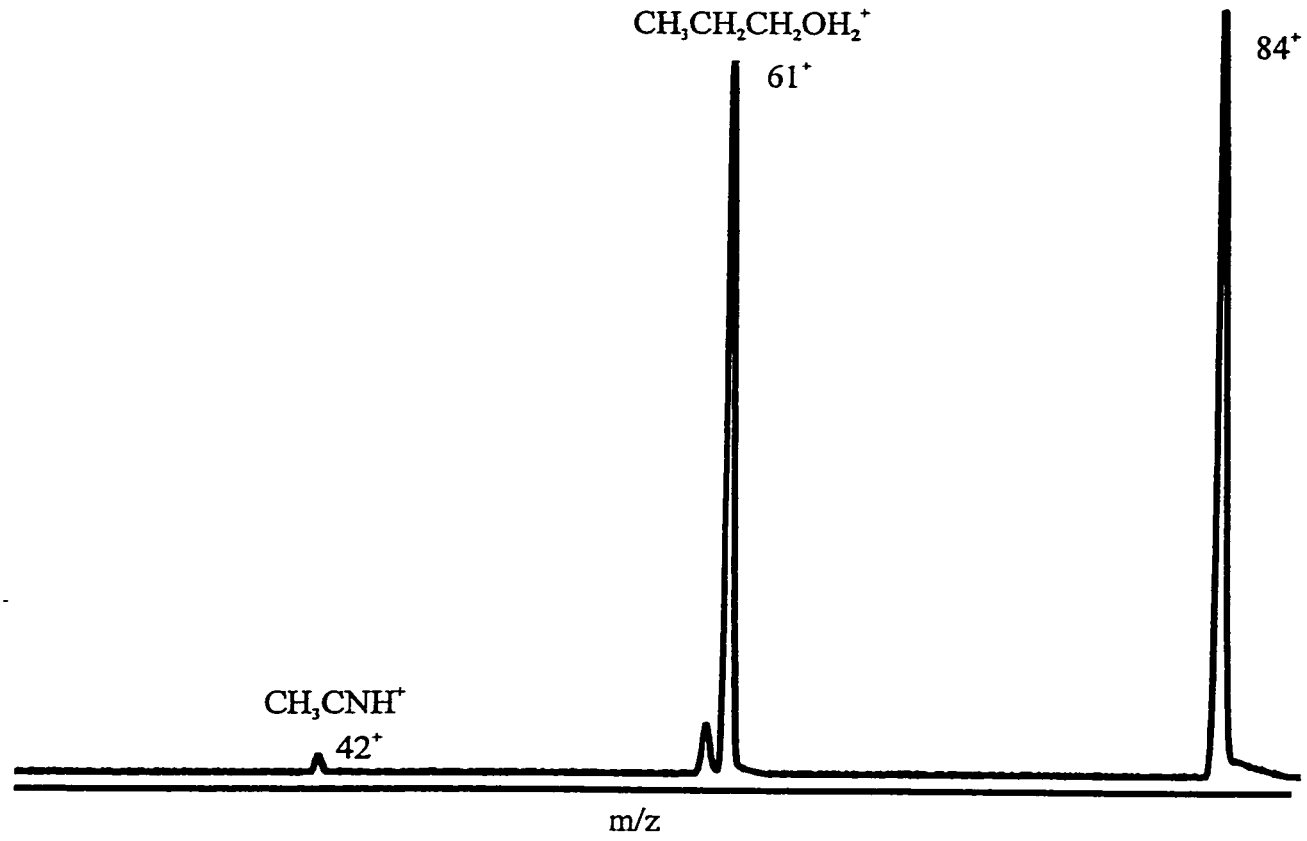

Fig 5.3.5 MI mass spectrum of the $(CH_3CN)(CH_3CH_2CH_2OH)H^+$ cluster ion.

5.4 Conclusion

A Finnigan GCQ ion trap mass spectrometer was used to measure the rate constants for three reactions between acetonitrile and alcohols (methanol, ethanol and n-propanol). The values were all significantly lower than those predicted from collision theory due to the presence of an isomerization reaction of the initially formed excited proton-bound dimer. The magnitudes of the isomerization barrier extracted from the kinetic data are consistent with an S_N2-type rearrangement of the dimer. The isomerization of nitrile/alcohol proton-bound dimers is believed

to take place by a mechanism similar to that predicted for the proton-bound alcohol dimers, namely an S_N2-type attack by CH_3CN on the alcohol carbon adjacent to the OH_2 moiety, eg. $[CH_3CN \bullet\bullet\bullet CH_3OH_2]^+$ [8]. The values for E_{iso} obtained in this study, when viewed *relative* to the activation energy for the simple dissociation, E_{diss}, are consistent with this type of mechanism. The cluster $(CH_3CN)(CH_3CH_2OH)H^+$ has the strongest hydrogen bonds due to the similarity in the PA values for acetonitrile and ethanol. Although the larger alkyl group should stabilize an intermediate $[CH_3CN \bullet\bullet\bullet CH_2(CH_3)OH_2]^+$ complex and the CH_3CH_2-OH_2^+ bond is weaker than the CH_3-OH_2^+ bond, the E_{iso} for the isomerization is larger for this cluster than for that involving methanol. If the S_N2 mechanism is valid, the strength of the H-bonding in the proton-bound dimer must result in a higher initial energy rearrangement to form $[CH_3CN \bullet\bullet\bullet CH_2(CH_3)OH_2]^+$. The value for k_{obs} is affected most by the relative values of E_{diss} and E_{iso} and so is still larger than that measured for the reaction involving methanol. It is noteworthy that the E_{diss} for the propanol-acetonitrile dimer is predicted to be lower than that for the ethanol-acetonitrile dimer. This may be an artifact of the MP2/6-31+G(d) level of theory as compared to the G2 levels used to calculate E_{diss} in the other two systems. It also means that the difference between E_{diss} and E_{iso} for this system may be underestimated.

References

[1] P. M. Mayer, J. Phys. Chem. A 103 (1999) 3687-3692.

[2] M. Meot-Ner, in Gas-Phase Ion Chemistry, M.T. Bowers (Ed), Academic Press, New York, 1979.

[3] T. Baer and W. L. Hase, Unimolecular Reaction Dynamics, Theory and Experiments, Oxford University Press, New York,1996.

[4] T. Su and W. J. Chesnavich, J. Chem. Phys. 76 (1982) 5183-5185.

[5] T. Su and M. T. Bowers, J. Chem. Phys. 58 (1973) 3027-3037.

[6] W. J. Hehre, L. Radom, P. v. R. Schleyer and J. A. Pople, Ab Initio Molecular Orbital Theory, Wiley, New York,1986.

[7] M. J. Frisch, G. W. Trucks, H. B. Schlegel, G. E. Scuseria, M. A. Robb, J. R. Cheeseman, V. G. Zakrzewski, J. A. Montgomery, R. E. Stratmann, J. C. Burant, S. Dapprich, J. M. Millam, A. D. Daniels, K. N. Kudin, M. C. Strain, O. Farkas, J. Tomasi, V. Barone, M. Cossi, R. Cammi, B. Mennucci, C. Pomelli, C. Adamo, S. Clifford, J. Ochterski, G. A. Petersson, P. Y. Ayala, Q. Cui, K. Morokuma, D. K. Malick, A. D. Rabuck, K. Raghavachari, J. B. Foresman, J. Cioslowski, J. V. Ortiz, B. B. Stefanov, G. Liu, A. Liashenko, P. Piskorz, I. Komaromi, R. Gomperts, R. L. Martin, D. J. Fox, T. Keith, M. A. Al-Laham, C. Y. Peng, A. Nanayakkara, C. Gonzalez, M. Challacombe, P. M. W. Gill, B. Johnson, W. Chen, M. W. Wong, J. L. Andres, C. Gonzalez, M. Head-Gordon, E. S. Replogle and J. A. Pople *GAUSSIAN 98 Rev. A.7*; Gaussian Inc.: Pittsburgh PA, 1998.

[8] R. A. Ochran, A. Annamalai and P. M. Mayer, submitted for publication.

[9] T. M. Miller, in CRC Handbook of Chemistry and Physics, R.C. Weast (Ed), CRC Press,

Boca Raton,1987.

[10] J. R. D. Nelson, J. D. R. Lide and A. A. Maryott, in CRC Handbook of Chemistry and Physics, R.C. Weast (Ed), CRC Press, Boca Raton, 1987.

[11] L. A. Curtiss, K. Raghavachari, G. W. Trucks and J. A. Pople, J. Chem. Phys. 94 (1991) 7221.

[12] E. P. Hunter and S.G. Lias, J. Phys. Chem. Ref Data 27 (1998).

Claims To Original Research

1. An ion trap mass spectrometer has been modified for the measurement of ion/molecule reaction rate constants [1,2].

2.a) New values for ion/molecule rate constants have been determined using the ion trap. Results obtained were comparable to those studied using other experimental methods. These results were then used to extract isomerization energy barriers [1,2].

[1] Julie A.D. McCormack and Paul M. Mayer, " Ion/Molecule Reaction Kinetics using a modified Finnigan GCQ ion trap mass spectrometer: The energetics of the dehydration of proton-bound alcohol dimers" Int. J. Mass Spectrom., submitted for publication.

[2] Julie A.D. McCormack and Paul M. Mayer, "The energetics of the dehydration of nitrile-alcohol proton-bound dimers from ion/molecule reaction kinetics" Int. J. Mass Spectrom, submitted for publication.